Progress in carbon-based electrocatalyst derived from biomass for the hydrogen evolution reaction

Qichang Wang [a,1], Rui Guo [a,1], Zhanghong Wang [b,1], Dekui Shen [a,*], Ran Yu [a,*], KaiHong Luo [c], Chunfei Wu [d], Sai Gu [e]

[a] Key Laboratory of Energy Thermal Conversion and Control of Ministry of Education, School of Energy and Environment, Southeast University, Nanjing 210096, Jiangsu, PR China
[b] College of Eco-Environmental Engineering, Guizhou Minzu University, Guiyang 550025, PR China
[c] Department of Mechanical Engineering, University College London, London WC1E 7JE, United Kingdom
[d] School of Chemistry and Chemical Engineering, Queen's University Belfast, Belfast BT7 1NN, United Kingdom
[e] Faculty of Engineering and Physical Sciences, University of Surrey, Guilford GU2 7XH, United Kingdom

ARTICLE INFO

Keywords:
Hydrogen evolution reaction
Biomass
Carbon material
Transition metal
Electrocatalyst

ABSTRACT

Hydrogen evolution reaction (HER) involving electrocatalytic process is established as a promising and non-pollution method for hydrogen production. The cheap alternatives of precious-metal electrocatalysts with high activity and robust stability is essential for the high-scale application of electrocatalytic hydrogen evolution. Recently, carbon-based electrocatalysts derived from biomass have attracted more and more attentions with thanks to their characteristics as low-cost, renewable, abundantly distributed and environmentally friendly. In this work, the original carbon material derived from biomass and the one doped with N and/or S as HER electrocatalysts are intensively overviewed regarding to the electrochemical performance and hydrogen yield. The overpotential at 10 mA cm^{-2} (η_{10}) is generally greater than 100 mV, which is far inferior to Pt-based catalysts. Consequently, biomass-based carbon materials decorated by transition metal and/or trace amount precious metal were introduced for improving the HER performance. The synergistic effect between metals and heteroatoms can significantly enhance the electrocatalytic activity, and the smallest value of η_{10} is 10 mV. The limitations and challenges in this area were also addressed as (1) the in-depth investigation of conversion and electrocatalytic mechanism, (2) metal modification via in-situ growth, (3) the reproducibility for biomass transformation, and (4) the catalyst assembly with renewable energy equipment.

1. Introduction

With the rapid development of human society, huge energy demand has been generated. The energy demand will reach 30 Terawatt (TW) in 2050 which is about 3 times than that of in 2010 [1]. Currently, fossils fuel still accounts for a very high proportion (about 79.5%, according to the statistics in 2018 [2]) in the human energy system. The consumption of fossils fuel such as coal, oil and nature gas has greatly promoted economic development [3]. Meanwhile, the heavy dependence of fossils fuels not only brought out energy crisis inevitably, but also seriously harmed the ecological environment [4]. To subject this problem and maintain long-term development, clean and sustainable energy has drawn extensive attention gradually. As an extraordinary alternative energy, hydrogen gas (H_2) has attracted world-wide concern of scientist for its high energy density and pollution-free. However, the actual industrial method of hydrogen production is mainly through steam reforming of fossil resources which will consume fossil fuels with low conversion and emit carbon dioxide (CO_2) [5]. An efficient, renewable and green method to achieve industrial generation of H_2 is urgency to further explore.

Consequently, water splitting through electrochemical which is an ideal reaction path to generate H_2 has been received widespread attention for its no emission and abundant raw material. The process of water splitting consists of hydrogen evolution reaction (HER) and oxygen evolution reaction (OER) as shown in Fig. 1a [6]. However, owing to the abnormally stable chemical structure of water molecule, a

considerable energy is needed to overcome the energy barrier, which is called overpotential in the electrochemical reaction (the value of η in Fig. 1a). Since the Platinum-group metal (PGM)-based catalysts and their derivatives have the optimal hydrogen bonding energy (HBE) and Gibbs free energy ($\triangle G_{H^*}$) for atomic hydrogen adsorption as shown in Fig. 1b, it have been regarded as the most active electrocatalyst for HER [7,8]. But the high-cost and source scarcity have greatly limited the application of PGM-based catalysts in large-scale H_2 production [9,10]. In addition, some obvious disadvantages such as gas poisoning, poor durability, metal corrosion and detrimental environmental impact also affected the use of PGM-based catalyst [11]. Hence, reducing noble metal loading or searching another efficient HER catalysts with low-cost, earth-abundant and stability is highly desirable.

According to the HBE data of different catalysts shown in Fig. 1b, scientists attempt to design a HER catalyst with use of transition metal (TM) such as nickel (Ni), cobalt (Co), molybdenum (Mo) etc. which generally existed as alloy or compounds in the process of catalyst construction [12–17]. However, the corrosion result from acidic or alkaline electrolytes will always affect the operation life and stability of such TM-based catalyst [6]. The agglomeration of TM-based catalyst during the electrocatalytic process is another restriction for the operation life and electrocatalytic activity toward HER. The inferior conductivity of some metal compounds also induces poor electronic transfer may limit the performance in HER [18–21].

It is a promising method to improve HER performance using the conductive carbon substrate as the support of TM-based catalyst [22,23]. The operation life and durability have been greatly upgraded with the protection of carbon substrate which can inhibit the corrosion from electrolytes and reduce the agglomeration of electrocatalyst nanoparticles [24–29]. The commonly used carbon support is graphene and carbon nanotubes which are expensive and cumbersome to synthesize. A simple, efficient, and green protocol with using of widely distributed raw materials to synthesize highly performance catalyst for hydrogen production is necessary.

As a well-known renewable energy source, the utilization of biomass is extremely limited and most of them have been combusted as a kind of fuel which will cause a waste of biomass and aggravate the air pollution [30]. It can be converted as the adsorption material, electrocatalyst, carbon support for catalysts and constructing the hybrid catalysts with the modification of metal compounds [31–36]. Such intrinsic properties of biomass can be summarized but not limited to the following aspects: (1) The biomass production usually involves to environmentally friendly processes with high quantity and quality, which provide reliable raw materials for carbon production by controlling the carbonization process [37], (2) The micro texture and multichannel structure in raw biomass can be designed as a natural electron transmission channel which will enhance the ability for ion diffusion/transport [38], (3) The morphological parameters such as size, shape and porosities are flexible to control in the process of structural and architectural design due to the adjustable carbonization process by alter the carbonization temperature or activator et al. [39], (4) Heteroatom, such as sulfur (S) (hair) [40,41], nitrogen (N) (peanut nodule) [42,43], and phosphorus (P) (phytic acid) [44,45] doped biomass-derived carbon material after carbonization is capable to manufacture lattice defects, expose more active sites, modify the electron acceptors-donors characteristics of carbon, regulate the density of states (DOS) near the Fermi level, et al., resulting in an better catalytic performance for hydrogen production [6,46–48], (5) Various functional groups on the surface of biomass such as C-O, COOH–, and –OH, et al. endow an immense space for the surface modification, further functionalization, and adjustment of physicochemical properties.

Recently, partial research has been reported on the electrocatalytic activity for HER using biomass-derived carbon material or the hybrid material of biomass-based carbon material and metal compounds. In this work, the nature of biomass-based catalyst is summarized, and the original biomass-derived carbon materials with heteroatom self-doped are intensively discussed. The work on the exogenous heteroatoms doped with biomass-derived carbon materials is introduced, followed by the biomass-based carbon material with the transition metal modification of TM and its compound. The synthesis protocols and functionalization approaches of various catalysts are also described, involving the relationship among the defective construction, active sites exposure, crystal structure and catalytic activity. Finally, the prospects, challenges, and development trends in the designing methods for biomass-derived carbon material used in HER are addressed.

2. Conversion methods for biomass-based carbon materials

Biomass is a widely-distributed carbon source for preparation of carbon materials via facile thermochemical methods (*i.g.*, thermal-treatment, hydrothermal, and activation). The functionalization and modification of biomass-based carbon materials can be achieved by using these synthesize methods. During the conversion process, the introduction of metal compound into the carbon framework could improve the electrocatalytic performance for the composite materials.

During the process of the biomass pyrolysis, the volatiles immersed in biomass were gradually released to introduce pores of hierarchical sizes into final carbon material. However, the porous, morphological, and physical–chemical properties of the carbon material was greatly influenced by the pristine structure of biomass species and the harsh operating conditions [49]. By using chemical activation method, the porosity and specific surface area of biomass-based carbon materials are significantly enhanced with the help of potassium hydroxide (KOH), magnesium chloride ($MgCl_2$), zinc chloride ($ZnCl_2$), etc. as the commonly-used activation reagent [4].

It is estimated that the original framework of biomass was demanded

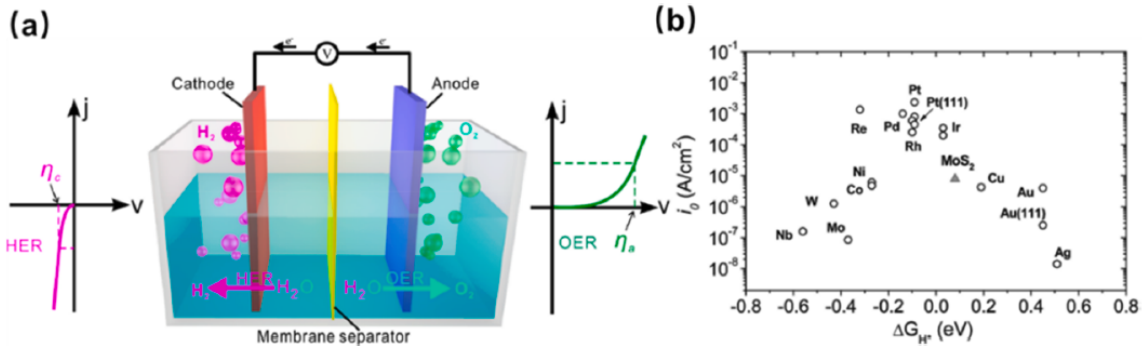

Fig. 1. **(a)** Hydrogen evolution reaction and oxygen evolution reaction of electrocatalytic water splitting. Adapted with permission [6]. Copyright 2019, American Chemical Society. **(b)** Volcano plot of the exchange current density as a function of the DFT (density functional theory)-calculated Gibbs free energy of adsorbed atomic hydrogen for different catalysts. Adapted with permission [7]. Copyright 2007, American Association for the Advancement of Science.

to be sustained due to its facilitation of the electronics transportation and electrocatalytic activity [38]. As a mild transformation process, hydrothermal is helpful for maintenance of the morphological structure of biomass during carbonization process, which can also be sustained in the post-calcination [50–52]. The hydrothermal method is also adopted to prepare carbon quantum dots, as another excellent electrochemical catalyst precursor [53].

In order to introduce metal compound into the carbon skeleton, the co-pyrolysis of biomass with metallic compound is well developed. The mixture of biomass and metallic compound prepared by mechanical co-grinding or impregnation was calcined at an elevated temperature [54,55]. The biomass was reacted with metal compound during the calcination process to produce the functional carbon materials. The metal loaded on the carbon skeleton in terms of nanocrystals of oxides, nitrides, and carbides etc. [56,57]. Hydrothermal carbonization process is another method to hold the metal ions on the solid product, distribution of the metal compound on which can be homogeneously distributed after the post-calcination [58].

3. Preparation of biomass-based carbon materials as electrocatalyst

Metal-free catalyst exhibited an inferior performance toward HER until Chen's group reported a high activity catalyst constructed by nanoporous graphene with N and S co-doped [46]. The coupling effects between heteroatom and lattice defects significantly promote the catalytic ability through the high conductivity resulting from electron-rich in defective structure and the optimized $\triangle G_{H^*}$ which is infinitely approaching to the Pt catalyst ($\triangle G^{NS\text{-}G}{}_{H^*}$=0.12 eV vs. $\triangle G^{Pt}{}_{H^*}$=0.09 eV) [46]. Hereafter, various heteroatom dual-doped graphene (such as S/N-G, P/N-G, etc.) has been investigated through DFT calculation and experiments. The electron acceptor–donor properties of graphene are modified with the synergistic coupling effect of two heteroatoms.[47]

The strategy of heteroatom doping can also be applied to the biomass-derived carbon material which may improve the HER property of the obtained carbon materials. Especially, the abundant heteroatom in biological component can form self-doped atom which can largely enhance the HER performance and reduce the use of chemical reagents. Furthermore, graphitized carbon materials with high conductivity will be obtained by high temperature treatment or catalytic graphitization [59–61]. Therefore, to construct the heteroatom self-doped graphitization carbon material is a promising catalytic choice. Moreover, doping with exogenous atoms from chemical reagents is another method of synthesizing heteroatom-doped biomass-based carbon material.

3.1. Carbon material with self-doping heteroatom

3.1.1. N-doped carbon material

Since N-containing organic components are the most common substances in biomass, it is so convenient to design of catalysts for N self-doped carbon materials using natural abundant biomass precursor such as plant [62,63], animal [64,65], microorganism [66,67], biomass extracts [68,69] and food waste [70,71]. Peanut shells are widely used as precursor for the fabrication of carbon materials and commonly utilized in the oxygen reduction or supercapacitors due to its rich N-containing [36,72]. However, few studies have reported its application toward HER. For the first time, Maduraiveeran's group demonstrated a facile two-step thermal-treatment to synthesize a multilayer carbon nanosheets (PSAC) from peanut shell waste which is consistent with the strategy of green chemistry [73]. In the second step, KOH as an

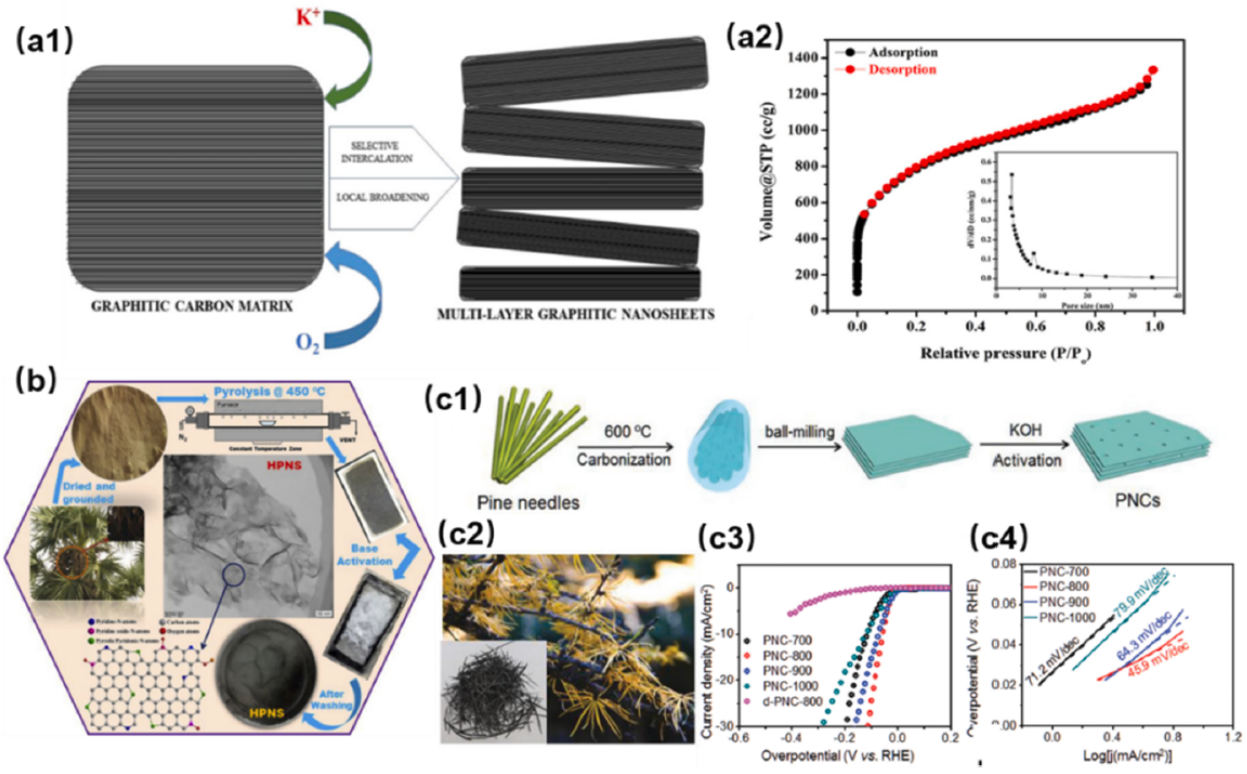

Fig. 2. **(a1)** Model for the activation mechanism by KOH in pyrolysis process in N_2 atmosphere, **(a2)** N_2 adsorption–desorption isotherm of PSAC (inset BJH pore distribution of PSAC). Adapted with permission [73]. Copyright 2019, Elsevier. **(b)** Graphical representation of synthesis of HPNS carbon from palm waste. Adapted with permission [11]. Copyright 2019, Elsevier. **(c1)** Schematic illustration of the synthesis process of PNCs, **(c2)** Photo of raw pine needles, **(c3)** LSV curves and **(c4)** corresponding Tafel plots of PNC samples for HER in 0.5 M H_2SO_4. Adapted with permission [83]. Copyright 2017, Royal Society of Chemistry.

activating agent was added in the residual carbon, the activation mechanism by KOH is shown in Fig. 2a1, it will significantly enhance the porosity, the formation of the defects sites and possibly affect the graphitization [74]. The multilayer and abundant mesopores endowed a high surface area of 2338 $m^2\ g^{-1}$ (Fig. 2a2). In addition, the ratio of the ratio of G band and D band (I_G/I_D) was 0.99 which suggested a defect-rich structure of PSAC [75,76]. The plentiful defect sites coordinated by N-containing component such as pyridinic, pyrrolic, graphitic and pyridine oxide nature of nitrogen atoms may increase the catalytic sites in the carbon structure [75]. Such superior characteristics leaded an excellent HER performance of PSAC in 0.5 M sulfuric acid (H_2SO_4). The onset potential is 80 mV (η_0) and the overpotential at 10 mA cm^{-2} is about 400 mV (η_{10}). The Tafel slope which indicates the mechanism and the rate-determining step of HER process is only 75.7 mV dec^{-1}, which is better than many previous reported catalysts [77–80].

Through a similar two-step thermal-treatment shown in Fig. 2b, Prabu and co-workers reported a N-doped graphene-like hierarchical porous nanosheets using the dry spathe-pollen waste of palm plant [11]. The synthesized hierarchical porous nanosheets (HPNS) owned a high surface area of 1297 $m^2\ g^{-1}$ and a higher ratio of I_G/I_D of 1.03. Furthermore, it is believed that the pyridinic, pyrrolic, and graphitic at defects will promote the H^+ adsorption/desorption during the HER process [81,82], which is consistent with the DFT results that the HPNS with N-doped has a more optimal HBE than undoped carbon (super P). In the investigation of HER in 0.5 M H_2SO_4, HPNS exhibited a small overpotential of 330 mv at 10 mA cm^{-2}, a low Tafel slope of 63 mV dec^{-1} as well as a durability of about 10 h. The double layer capacitance (C_{dl}) which is related to the electrochemical active surface area (ECSA) was also studied through cyclic voltammetry (CV) at a non-Faradaic process. The relative high ESCA value of 61.4 $cm^2\ g^{-1}$ through the calculation from C_{dl} value (7.86 mF cm^{-2}) is another reason for the high HER performance.

Zhu et al. synthesized a microporous N-doped carbon framework (PNC) with pine needles [83]. As shown in Fig. 2c1 and c2, pine needles were firstly pre-carbonized at 450 °C, followed by a ball-milling for 30 mins and finally with the activation of KOH at a range of 700 ~ 1000 °C (PNC-T, T = 700 ~ 1000 °C). The PNC-800 showed the best HER electroactivity in 0.5 M H_2SO_4 with a small onset potential of 4 mV, a overpotential of 62 mV at 10 mA cm^{-2} and a quite small Tafel slope of 45.9 mV dec^{-1} (Fig. 2c3 and 2c4), all of them are comparable to the commercial Pt/C. Notably, the physical–chemical properties of PNC-800 are not the best among PNC-T. With the increase of pyrolysis temperature, the specific surface area of PNC-900 is larger than that of PNC-800 (2433 $m^2\ g^{-1}$ vs. 1931 $m^2\ g^{-1}$), but the electrocatalytic activity of PNC-900 is poor. This may attribute to the decrease in the ratio of I_G/I_D (0.96 vs. 0.93), nitrogen content (1.4 at% vs. 1.1 at%), and the value of C_{dl} (2.4 mF cm^{-2} vs. 1.1 mF cm^{-2}). Furthermore, the PNC-1000 leaded the most inferior catalytic activity resulting from the sharply decrease of the ratio

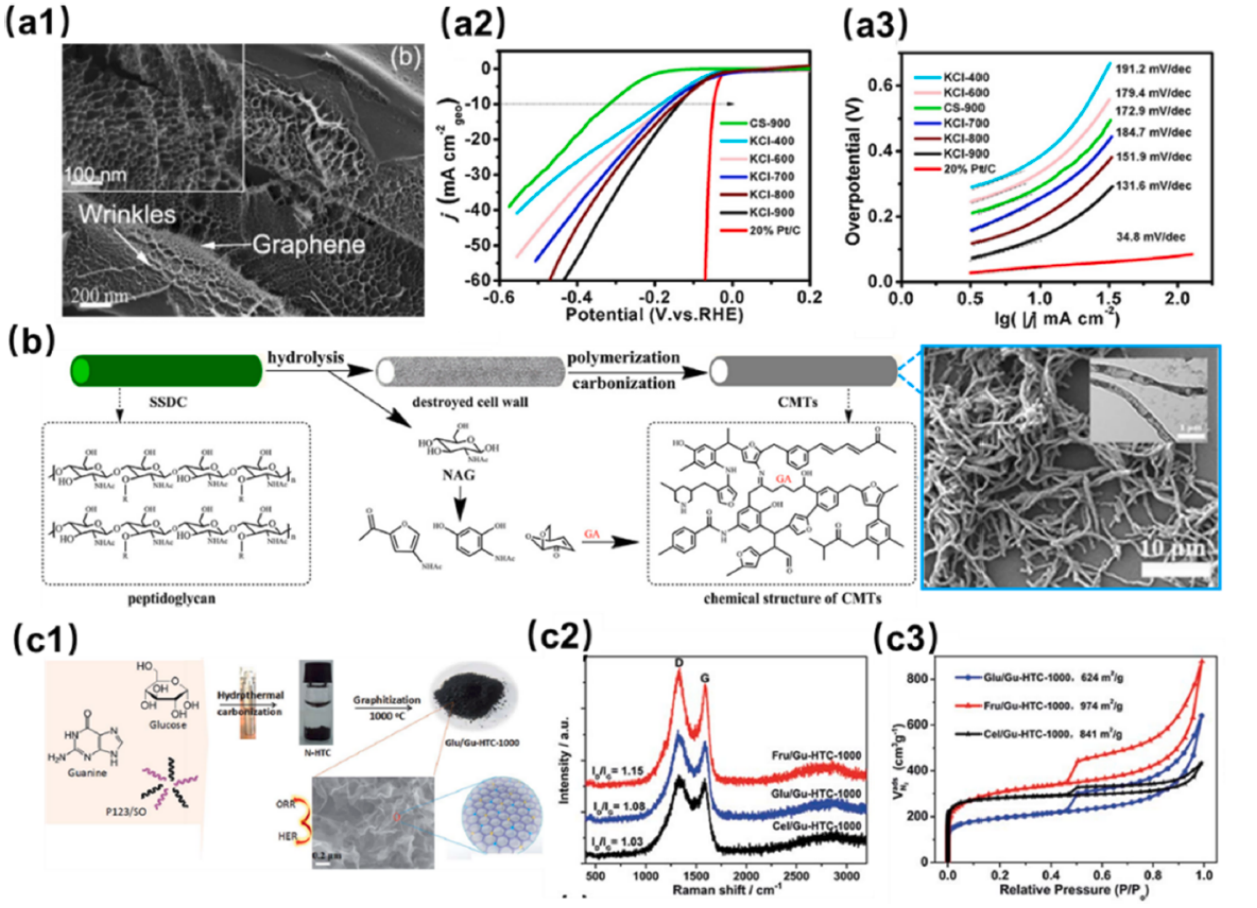

Fig. 3. **(a1)** FE-SEM images of KCI-900 samples, **(a2)** Polarization curves and **(a3)** Tafel plots of CS-900, KCI-900, KCI-800, KCI-700, KCI-600, KCI-400 and 20% Pt/C catalysts in N_2-saturated 0.5 M H_2SO_4 solution, respectively. Adapted with permission [84]. Copyright 2016, Elsevier. **(b)** Possible mechanism for the formation of CMTs and the SEM/TEM images of CMTs. Reproduced with permission [85]. Copyright 2016, Elsevier. **(c1)** The synthetic route of Glu/Gu-HTC-1000, **(c2)** Raman spectra and **(c3)** nitrogen adsorption/desorption isotherms of Fru/Gu-HTC-1000, Glu/Gu-HTC-1000 and Cel/Gu-HTC-1000 respectively. Adapted with permission [86]. Copyright 2017, Royal Society of Chemistry.

of I_G/I_D value (0.43). The high graphitization of carbon materials can be achieved by high temperature, while the disordered carbon and defect sites will also be seriously reduced. Hence, it is critical for the carbon material to control the degree of disorder and graphitization.

Silk cocoon is a common raw material in apparel industries. Through a one-step thermal carbonization process with potassium chloride (KCl) activation, Liu et al. designed a honeycomb-like carbon nanosheets (KCl-T) consisted of microporous and multilayers structure as depicted in Fig. 3a1 [84]. The extraordinary performance of HER in 0.5 M H_2SO_4 was achieved when the pyrolysis temperature is 900 °C (KCl-900) due to the rich N-containing of 4.7 at%, low charger resistance of 19.99 Ω and high ratio of I_D/I_G of 1.06. Hydrogen evolution occurred at an onset overpotential of 63 mV (Fig. 3a2). When the current density reached 10 mA cm^{-2}, the overpotential is 137 mV. In addition, a slightly higher Tafel slope of 132 mV dec^{-1} (Fig. 3a3) and a fine durability of more than 10 h was obtained.

It is accessible for hydrothermal carbonization (HTC) protocol to obtain the functional carbons by maintaining of original structure of biomass precursor. With natural micro-tubular structure of Streptomyces sporoverrucosus dwc-3 (S. sproroverrucosus dwc-3) (Fig. 3b), it was chosen for the first time as the carbon precursor for a low temperature HTC research by Li et al.[85]. After low temperature HTC at 180 °C, the intrinsic micro-tubular of S. sproroverrucosus dwc-3 was inherited by carbon-based microtubes (CMTs). The diameter ranges from 400 to 500 nm, as well as a wall thickness of about 50 nm. The electrochemical study in 0.5 M Na_2SO_4 + 0.1 M H_2SO_4 electrolyte showed that the prepared CMTs owns a high electrocatalytic activity for HER.

The HTC carbon still has obvious drawbacks of low porosity and large particle size which is not sweet for electrocatalyst. The biomass-derived carbon material via HTC needs further functionalization. Therefore, Huang et al. reported a 2 dimensional (2D) morphology of crystalline carbons via HTC method combined with high temperature pyrolysis as shown in Fig. 3c1 [86]. They integrated abundant nitrogen atoms, developed porosity and 2D morphology into carbon frameworks by using biomolecule guanine and diverse carbohydrates (glucose, fructose and cellulose) as carbon precursors. As illustrated in Fig. 3c2, the high I_D/I_G values (1.15) showing a defect rich structure in the flawless carbon skeletons. The nitrogen content of 2.39 at% and porous nitrogen doped carbon with high specific surface area of 974 $m^2\ g^{-1}$ were obtained by further high temperature carbonization (Fig. 3c3). The Fru/Gu-HTC-1000 catalyst required a 350 mV overpotential to drive a current density of 10 mA cm^{-2} in 1.0 M KOH, which is better than most other equivalent benchmarks as well as Pt-based electrocatalysts.

It is economical and environment-friendly to utilize the food waste as a kind of precursor for carbon material. As shown in Fig. 4a1, the N-doped porous carbon material (NPCSBF) from Chinese steamed bread flour through successive hydrothermal treatment and pyrolysis was successfully proposed by Nsabimana et al. [87]. The hydrothermal treatment tremendously promoted the strength of NPCSBF which enabled the manufacturing of robust monolithic N-doped porous carbon. Due to the high strength and integration, NPCBSF was applied to prepare a self-support electrode. It showed an excellent HER performance in 0.5 M H_2SO_4 with a relatively low overpotential of ~ 220 mV at 10 mA cm^{-2} and a Tafel slope of ~ 77 mV dec^{-1} which mainly ascribed to the higher value of C_{dl} (140.24 mF cm^{-2}) (Fig. 4a2 and a3). The NPCSBF modified electrode exhibited a nearly 100% Faradaic efficiency and a robust stability for more than 11 h.

Prabu et al. developed a facile two-step thermal-treatment with the activation of KOH to construct a 2D hierarchical carbon nanosheets (NACS) from Indian Ooty Varkey (IOV) food waste (Fig. 4b) [88]. The inter-tuned sheets and micro/mesopores structure with a high specific surface area of 1478 $m^2\ g^{-1}$ was founded in NACS. The ratio of I_D/I_G is 1.03 from the detection of Raman spectra which suggested a defect-rich structure in NACS. The NACS required a 380 mV overpotential to drive a current density of 10 mA cm^{-2} in 1.0 M KOH and the Tafel slope is 85 mV dec^{-1}.

The ideal HER electrocatalysts owns near zero value of $\triangle G_{H^*}$, while the N-doping adjusts the band structure and electronic properties of biomass-derived carbon materials which will approach the $\triangle G_{H^*}$ value to zero and thus affect the adsorption behaviors of H atoms. Especially, the pyridinic-N and pyrrolic-N in carbon lattice significantly favors the adsorption of H atoms to promote the HER performance of N-doped carbon materials [89]. Hence, to synthesize the self-doped heteroatoms of N through N-containing biomass is a superiority for biomass-derived carbon. The pyridine-N and pyrrolic-N are two kinds of N-atoms doping forms for promoting the electrocatalytic performance of biomass-derived carbon. It needs to be noted that the conversion of N atoms is

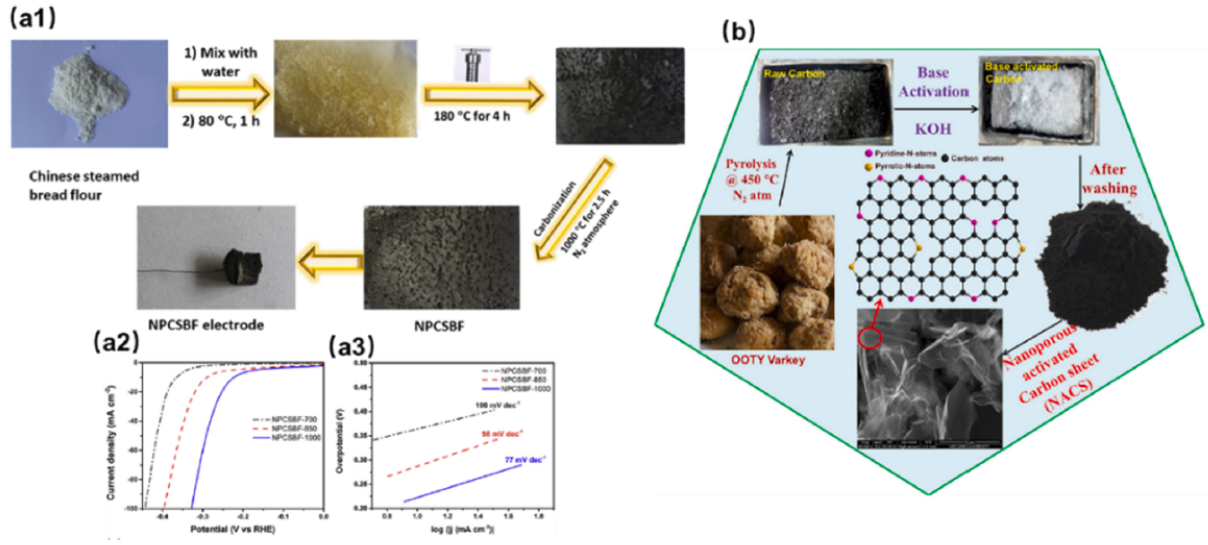

Fig. 4. **(a1)** Schematic representation of the synthesis of NPCSB, **(a2)** polarization curves of NPCSBF-1000, NPCSBF-850, and NPCSBF-700 in 0.5 M H_2SO_4 and **(a3)** corresponding Tafel plots. Adapted with permission [87]. Copyright 2018, Elsevier. **(b)** Pictorial representation of the synthesis of NACS. Adapted with permission [88]. Copyright 2018, Elsevier.

complicated, leading to the difficulty for controlling the oriented conversion of N-atoms to the aforementioned forms. The conversion mechanism for self-doped N-atoms is critical to prepare functional carbon materials with high catalytic activity.

3.1.2. N and S co-doped carbon material

Compared with the single-atom-doped graphene, the dual-doped ones exhibited more incredible performance in HER resulted from the more appropriate H* adsorption [78]. Through the theoretical calculations, a small $\triangle G_{H^*}$ value of 0.23 eV was obtained with S and N dual-doped graphene, which is much lower than the N single-doped graphene (0.81 eV) [47]. Accordingly, the S and N co-doped carbon material derived from biomass may possess similar properties which can improve the electrocatalyst activity.

By taking advantage of the rich elemental properties of the peanut root nodules, Zhou and co-workers prepared the S and N co-doped carbon nanosheets (RN-800) through one-step thermal decomposition of peanut root nodules with the activation of $MgCl_2$ [90]. Through the HER investigation in 0.5 M H_2SO_4, the obtained RN-800 showed an excellent HER performance compared to the other reported HER catalysts [91–93]. The onset potential is only 27 mV, along with a small overpotential of 116 mV at 10 mA cm^{-2} (Fig. 5a1). The Tafel slope is 67.8 mV dec^{-1} (Fig. 5a2). In addition, RN-800 has a larger current density of 59.4 mA cm^{-1} at 200 mV and a robust electrochemistry stability of more than 12 h (Fig. 5a3). The electric density surrounded S and C atoms was increased with the modification of S dopants compared with the N-doped carbon skeleton which may resulted in a better electrocatalytic activity of RN-800. Followed by the demonstration of DFT calculation as shown in Fig. 5a4, the S atoms play an important role in the HER activity promotion.

Considering the richness of nitrogen and sulfur content in human hair, Zhou's group reported a S, N co-doped porous carbon (HPC-800) via two-step pyrolysis [94]. The $ZnCl_2$ as a chemical activation agent was mixed with the pre-carbonized hair pieces in the second process of pyrolysis. Since the specific surface area and sulfur content is more than RN-800 (820 $m^2\ g^{-1}$ vs. 513.3 $m^2\ g^{-1}$; 4.9 at% vs. 0.27 at%) [90], HPC-800 showed more satisfactory performance toward HER with a smaller onset overpotential of 12 mV, a current density of 10 mA cm^{-2} at 100 mV, as well as a Tafel slope of 57.4 mV dec^{-1}. Moreover, a higher stabilized current density was acquired compared with commercial Pt/C at same voltage (450 mA cm^{-2} vs. 300 mA cm^{-2}).

Compared to the N-doped carbon materials, the N/S dual-doped carbon materials exhibited the high activity for HER with a relatively suitable H* adsorption. The combination of positivity charged N dopants and negatively charged S dopants at a lattice defect provides a fast electron transfer path for HER. The interplay of N and S dopants with geometric lattice defects resulting in the superior electrocatalytic activity of HER [6]. In addition of N, S co-doped carbon materials, other non-metal element such as phosphorus, boron in biomass was potential for being converted to dopants due to its modification on the hydrogen bonding energy. Therefore, the forms of these heteroatoms played an important role in improving the electrocatalytic performance for HER.

3.2. Carbon material doped with exogenous atoms

The exogenous atoms doping with additive of commercial chemical reagent is another method to manufacture the heteroatom doped carbon catalysts. The exogenous atoms loaded on the carbon skeleton can improve the amounts and species of the heteroatoms in biomass macromolecules. Hence, a graphene-like sheets (NHPCF) from natural cattail fibres was designed by Liu et al. via a chemical activation and N atom modification treatments as illustrated in Fig. 6a1 [95]. Natural cattail fibres were firstly grounded with potassium bicarbonate ($KHCO_3$) and then calcinated at 900 °C. Subsequently, the rinsed porous carbon was mixed with hot melamine solution and hydrothermal reaction was carried out at 100 °C for 320 mins. The obtained compound was

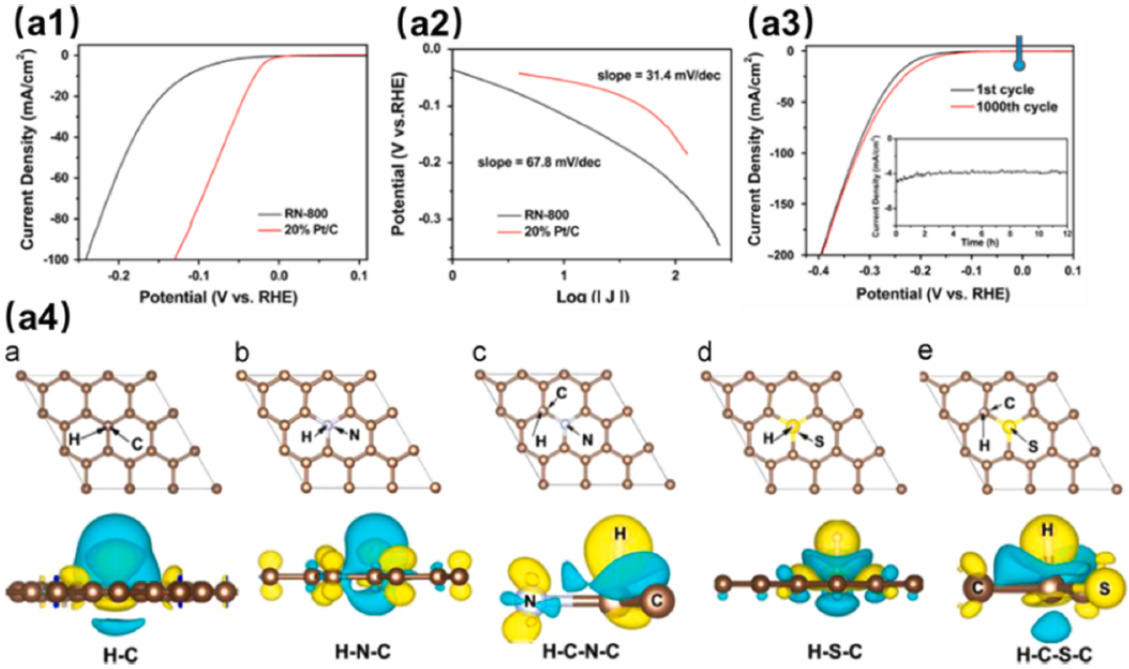

Fig. 5. **(a1)** Polarization curves for HER of RN-800 and 20 wt% Pt/C in 0.5 M H_2SO_4 with sweep rate 5 mV/s, **(a2)** Corresponding Tafel plots derived from **(a1)**, **(a3)** HER polarization curves for RN-800 before and after 1000 cycles of potential sweeps. Inset shows the current–time plot at the applied potential of −0.25 V (vs. RHE), **(a4)** Structural models and charge density of H adsorbed on the surface of graphene, N-doped graphene and S-doped graphene. **(a4a)** H atom was combined on the C atom; H atom was combined on the N **(a4b)** or S **(a4d)** dopant atom; H atom was combined on the C atom around N **(a4c)** or S **(a4e)** dopant atom. The blue and yellow symbols denote decreased and increased charge density, respectively. Adapted with permission [90]. Copyright 2015, Elsevier. (For interpretation of the references to colour in this figure legend, the reader is referred to the web version of this article.)

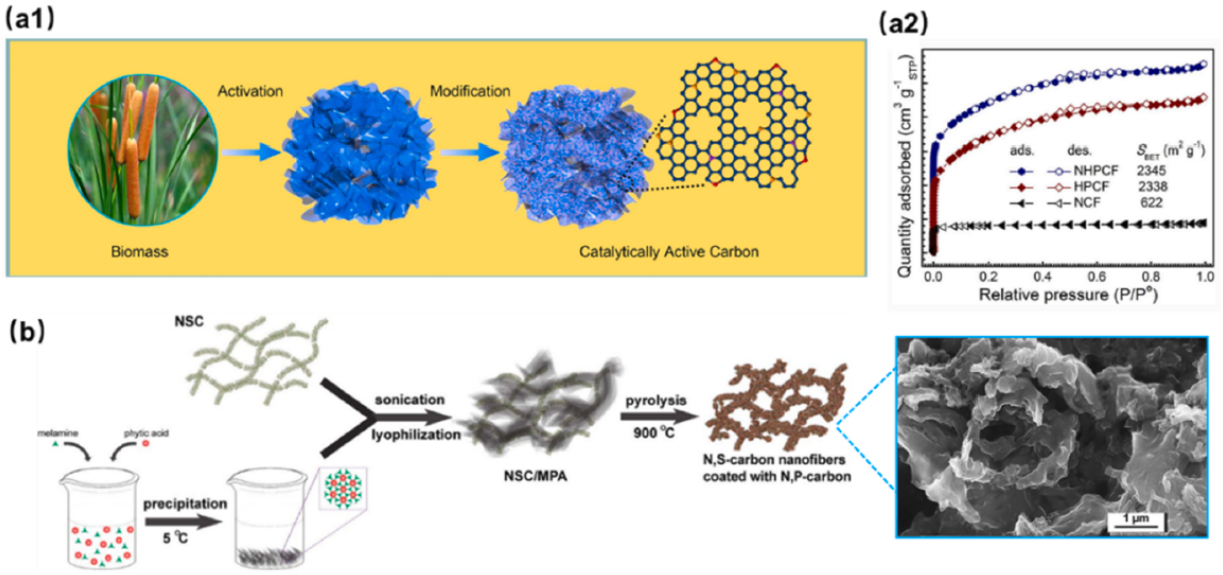

Fig. 6. **(a1)** Preparation of NHPCF from cattail spikes, **(a2)** Nitrogen adsorption–desorption isotherms calculated by NLDFT method of NCF, HPCF, and NHPCF. Adapted with permission [95]. Copyright 2019, Elsevier. **(b)** Carbon hybrids preparation. Adapted with permission [96]. Copyright 2017, Elsevier.

annealed at 400 °C for 2 h, then heated to 500 °C at a temperature increase rate of 2.3 °C min^{-1}, and then maintained for 3 h. The NHPCF displayed a relatively high specific surface area of 2345 m^2 g^{-1} (Fig. 6a2) due to the hierarchical pores structure. HER test in 0.5 M H_2SO_4 showed the onset potential is 80 mV, the overpotential at 10 mA cm^{-2} is 150 mV and the Tafel slope is 89 mV dec^{-1}.

As shown in Fig. 6b, Mulyadi and co-workers prepared a N, S, and P tri-doped 3D carbon architecture using the cellulose nanofibrils through solvothermal and pyrolysis [96]. During solvothermal treatment, N, S co-doped carbon fibers (NSC) was firstly obtained which the N and S atoms originated from ammonium thiocyanate. Then, NSC was mixed with the melamine-phytic acid (MPA) to form NSC/MPA suspension by a sequential step of incubating, centrifugal treatment and re-dispersing. Finally, the N, S co-doped carbon fibres coated with the N, P co-doped carbon nanoparticles (NSC/MPA-5) was obtained after a two-step thermal-treatment. Although the hybrid material exhibited a comparable activity with Pt/C toward ORR, the HER performance is relatively inferior. The onset potential is up to 233 mV, while the overpotential of 331 mV was required to drive a current density of 10 mA cm^{-2}.

The nature of biomass-based electrocatalysts derived from biomass have been discussed above. The dopant with heteroatoms greatly affected the electroactivity for HER by constructing more defects, exposing more active sites and optimizing the value of $\triangle G_{H^*}$, etc. Table 1 has shown the parameters associated with the electrocatalyst activity and HER performance. As one can see, most of the electrocatalysts derived from biomass with the dopant of N atom have a relatively higher overpotential (over 130 mV) to obtain a current density of 10 mA cm^{-2}. There is only the pine needle derived carbon materials exhibited the most active electrocatalytic for HER, which have the lowest value of η_{10} of 62 mV, together with a smallest Tafel slope of 45.9 mV dec^{-1} [83]. The biomass-based carbon materials with the N and S co-doped presented better HER performance with a smaller η_{10} which is lower than 120 mV [90,94]. However, the HER performance of this kind of electrocatalysts are far inferior to commercial Pt/C because the overpotential to drive the current density to 10 mA cm^{-2} of Pt/C is lower than 40 mV in 0.5 M H_2SO_4. The biomass-derived carbon material should be further functionalized and modified to approach, or even exceed, the electrocatalytic activity of Pt/C. The oriented conversion of various dopants was demanded during the preparation of biomass-based HER electrocatalyst.

4. Metal-involved modification of biomass-based electrocatalyst

Carbon materials modified with TM showed considerable activity for HER [97–101]. This result is attributed to the fact that the more appropriate HBE of TM compared with carbon material [6]. Therefore, the preparation of HER catalysts using TM or its compounds on biomass-derived carbon materials may be an effective method. The natural-rich structure for biomass makes it can be designed to obtain carbon materials with particular morphology (sphere, tube, et al.) and excellent physical–chemical properties via simple preparation protocol. Meanwhile, the micro texture and multichannel structure in raw biomass can be designed as a natural electron transmission channel which will enhance the ability for ion diffusion/transport, thereby promote the efficiency of hydrogen evolution. Furthermore, the surface functional groups of biomass derived carbon endow its more easily to coordinate with the metal ions during the synthesized process. The well-distributed heteroatoms (N, S, P et al.) doped in the skeleton of biomass-derived carbon can be introduced without chemical agents. Moreover, the self-doped heteroatoms not only adjust the electronic and band structure, but also can hybrid with metal compounds to form nitrides, sulfides, phosphides et al. Moreover, biomass-derived carbon materials as substrate can protect TM from corrosion of the electrolyte, thereby extending the operation life of the synthesis catalyst.

4.1. Tungsten (W)

W and its compounds have been widely explored as active catalysts toward HER due to its satisfactory structural and electronic properties [102,103]. Since carbon atoms are embedded in the W lattice, a "Pt-like" d-band electron density is formed [104–106]. Therefore, tungsten carbide (W_2C and WC) is similar to Pt in catalytic performance. Tungsten carbide and its compounds have shown effective surface catalysis in many research fields such as methanol oxidation, cellulose conversion and water reduction, etc. [107–109]. Meng and co-works reported WSoy catalysts by sintering ammonium tungstate (AMT), soybean powder and graphene nanoplatelets (GnP) [56]. Specifically, the mixtures of soybean powder and AMT were firstly added into deionized (DI) water and

Table 1
Comparison of HER performance of HER catalysts synthesized by biomass precursor.

Catalyst	Method	Biomass source	S_{BET}(m^2 g^{-1})	I_D/I_G	ECSA (mF cm-2)	Electrolyte	Mass loading (mg cm^{-2})	[a]Overpotential (mV), *η10*	Tafel slope (mV dec^{-1})	Refs
Biomass-based carbon materials as electrocatalyst										
N-doped carbon material										
PSAC	pyrolysis	peanut shells	2338	0.99		0.5 M H_2SO_4	0.95	400	75.7	[73]
HPNS	thermal treatment	palm waste	1297	1.03	7.86	0.5 M H_2SO_4	–	330	63	[11]
PNC-800	thermal treatment	pine needles	1931	–	2.4	0.5 M H_2SO_4	0.35	62	45.9	[83]
KCl-900	thermal carbonization	silk cocoon	349.3	>1.05	–	0.5 M H_2SO_4	–	137	131.6	[84]
Fru/Gu-HTC-1000	hydrothermalcarbonization	guaninecarbohydrate	974	1.15	–	0.1 M KOH	0.45	350	108	[86]
NPCBSF	hydrothermal treatment/ pyrolysis	Chinese steamed bread flour	–	–	140.24	0.5 M H_2SO_4	/	220	77	[87]
NACS	thermal treatment	Indian Ooty Varkey (IOV) food waste	1478.0	1.03	–	0.5 M H_2SO_4	0.519	380	–	[88]
N and S co-doped carbon material										
RN-800	thermal treatment	peanut root nodules	513.3	>1.1	27.4	0.5 M H_2SO_4	0.285	116	67.8	[90]
HPC-800	pyrolysis	human hair	830.0	1.07	7.2	0.5 M H_2SO_4	0.285	100	57.4	[94]
Carbon material doped with exogenous atoms										
NHPCF	thermal treatment	cattail fibers	2345	1.14	/	0.5 M H_2SO_4	0.417	150	89	[95]
NSC	solvothermal/pyrolysis	cellulose/ phytic acid	682	0.88	24.4	0.5 M H_2SO_4	0.25	331	99	[96]
Metal-involved modification of biomass-based electrocatalyst										
Tungsten (W)										
$WSoy_{0.7}GnP_{1.0}$	sintering	soybean	–	–	49.0	0.1 M $HClO_4$	10	105	36	[56]
WO_3/B-AC	sonochemical reaction/ pyrolysis	neem leaves	–	0.9	11.96	1 M KOH	–	360	14	[114]
Cobalt (Co)										
Co_3O_4/NCMT-800	pyrolysis	willow catkin	470.1	0.92	–	1 M KOH	1	210	–	[115]
CoOx@CN	sol–gel method/ calcined	glucosamine hydrochloride/glucose	311	–	37.4	1 M KOH	0.42	232	115	[57]
Co/ CoO@Co–N-C-800	hydrothermal/pyrolysis	shrimp-shell	647.7	–	–	0.1 M KOH	0.305	~343	–	[121]
Co-CoO/BC yolk-shell	impregnation/pyrolysis	holly leaves	926.2	–	–	0.5 M H_2SO_4	–	~210	–	[122]
Co_9S_8@NPC	molten-saltcalcination/ phosphorization	shrimp shell	278.6	0.98	–	1.0 M KOH	–	261	101.8	[123]
CoP/NPCFs	pyrolysis /thermal decomposition	sodium alginate	44.32	0.94	–	0.5 M H_2SO_4	–	135	67	[126]
CoP@C-NPs/ GA-5	sol–gel/ phosphorization	sodium alginate	–	1.03	55.83	1.0 M KOH	–	225	66	[127]
CoP/BMHNC	solvent thermal/Calcined	cinnamomum platyphyllum leaves	–	–	–	0.5 M H_2SO_4	0.30	95.8	33	[128]
Co_2P – C	hydrothermal/thermal treatment	yeast particles	632.8	<1	124.1	0.5 M H_2SO_4	–	96	34	[58]
Co-Co_2P@NPC/ rGO	hydrothermal/thermal treatment	Saccharomycete cells	110.2	–	9.9	0.5 M H_2SO_4	0.357	61.5	50.64	[50]
Co_2P	hydrothermal/ carbonization	spirulina	243.9	0.95	12.27	0.5 M H_2SO_4	0.357	181	55	[129]
Molybdeum (Mo)										
Mo_2C QDs/ NGCL	solid-statereaction	chitosan	–	1.05	55.2	0.5 M H_2SO_4	–	134	68.4	[137]
Mo_2C@S-CA	freeze-drying/ thermal treatment	cellulose	–	–	–	0.5 M H_2SO_4	0.48	176	66	[138]
Mo_2C@N-CNFs	freeze-drying/ pyrolyzed	bacterial cellulose	81.98	–	11.34	0.5 M H_2SO_4	1.02	167	70	[54]
Mo_2C/C	solid reaction	glucose	259	~1	38.6	0.5 M H_2SO_4	0.286	114	52	[55]
NP-Mo_2C/ PCMS	hydrothermal/freeze-drying/ annealing	red jujube	188	–	39.7	1.0 M KOH	–	80	46	[146]
Mo_2C@SNC	calcination	sunflower seeds	392.9	1.0	6.31	1.0 M KOH	2.47	60	71	[147]
Mo_2C	anaerobic pyrolysis/annealed	birch tree	80	–	18.6	0.5 M H_2SO_4	1	35	25	[150]

(*continued on next page*)

Table 1 (*continued*)

Catalyst	Method	Biomass source	S_{BET}(m^2 g^{-1})	I_D/I_G	ECSA (mF cm-2)	Electrolyte	Mass loading (mg cm^{-2})	[a]Overpotential (mV), *η10*	Tafel slope (mV dec^{-1})	Refs
DAC/MoS_2	activation/hydrothermal/ grinding	diospyros melanoxylon leaves	1509	–	–	0.5 M H_2SO_4	–	–	84	[155]
MoS_2/BCTM	hydrothermal/calcined	green celery	–	–	–	0.5 M H_2SO_4	0.159	176	51	[158]
MoP/CF	pyrolysis	sodium alginate	22.9	–	–	0.5 M H_2SO_4	0.36	200	56.4	[164]
Mo_1Soy	ultra-sonicated/ calcined	soybeans	5.2	–	–	0.1 M $HClO_4$	0.47	109	62.7	[168]
MoCot	hydrothermal/ annealing	sterilized cotton	63	–	–	0.5 M H_2SO_4	–	167	67	[169]
Nickel/Iron (Ni/Fe)										
PC-$Ni_{0.75}$	hydrothermal/ pyrolyzed	carrot	216	0.96	81.8	0.1 M KOH	–	297	134.9	[171]
NiOx-AC-500	thermal/ultrasonic	cauliflower leaves	1133	1.04	–	0.1 M KOH	–	180	121	[173]
NiP-800	Ni treatment	filter paper	–	<1	–	0.5 M H_2SO_4	–	–	45	[174]
CW-CNT@NC-NiFe	heat shock treatment	natural wood	–	–	–	0.5 M H_2SO_4	–	59	52.8	[179]
NiP/ Poplarwood	activation/plating	poplar wood	–	–	24.1	1.0 M KOH	–	83	73.2	[180]
FeP NPs@NPC	pyrolysis	phytic acid	–	1.04	–	0.5 M H_2SO_4	1.4	130	67	[184]
Ni-NiP@NPC/ rGO)	hydrothermal/calcination	Saccharomyc-ete cell	230.34	–	13.57	1.0 M KOH	–	< 100	57.93	[51]
P-Fe_3N@NC NSs/IF	annealing	Saccharomyc-ete cell	–	–	18.61	1.0 M KOH	–	102	32.93	[185]
Fe_3O_4/NCMTs (IL)	pyrolysis	catkins	530.41	1.08	–	1.0 M KOH	1	170	–	[193]
$Ni_{0.25}Fe_{0.75}$-N, P, S	annealing	alfalfa	121.2	0.85	4.4	1.0 M KOH	0.13	250	84	[200]
NF-8-A	pre-carbonized/pyrolysis	duckweed	116.5	1.49	28.1	1.0 M KOH	–	106	90	[201]
Platinum-group (Pt/Ru)										
G-ABC(Pt)	thermal treatment	turf grass	1201	–	–	1.0 M H_2SO_4	–	–	–	[202]
1% Pt@AC	pyrolyzed	areca leaves	388	–	–	0.5 M H_2SO_4	–	–	–	[203]
Mo_2C@Ru	annealing	corns	274.9	–	–	0.5 M H_2SO_4	0.275	24.6	58.4	[212]
Ru@CQDs	hydrothermal/ annealed	ginkgo leaves	–	<1	67.24	1.0 M KOH	–	10	47	[222]
Ru@CQDs	hydrothermal/ annealed	porphyra	–	0.95	–	1.0 M KOH	0.42	65	63	[223]
RuCo@CQDs	hydrothermal/ annealed	poplar leaves	–	1.16	52.3	1.0 M KOH	0.42	16	56	[224]
n-Pd@NDCDs	hydrothermal	M. citrifolia fruit	–	0.59	0.06	0.5 M H_2SO_4	0.05	291	135	[225]
Pd/VSAC	chemical activation /Oleylamine- mediated synthesis	vine shoots	1689	–	–	8 M KOH	0.57	224	144	[226]
0.5Rh-GS1000	calcination	guanine	344.3	–	39.3	0.5 M H_2SO_4	0.72	40	26	[229]
Rh/Ni@NCNTs	calcination	dglucosamine hydrochloride	121.2	–	35	1 M KOH		14	37.2	[230]
Rh_2P/NPC	calcination/phosphorization	starch	223	0.97	41.3	1 M KOH	0.78	17	32	[231]
Ag-WO_3 CSNSs	hydrothermal/ calcination	glucose	–	–	54.92	0.5 M H_2SO_4	3.6	207	52.4	[232]
P-Ag/NC	thermal annealing	glucose	–	–	–	0.5 M H_2SO_4	0.8	78	107	[233]
Au@NC	bioreduction/calcination	pycnoporus sanguineus	–	~1	18.65	0.5 M H_2SO_4	0.357	130	76.8	[234]

a) The overpotential (η_{10}) is given with respect to reversible hydrogen electrode (RHE)

ultrasonicated for 40 mins to form uniform suspensions. After dried at 90 °C for overnight, the dried powders were mixed with GnP and sintered at 850 °C in argon (Ar) for 2 h to obtain $WSoy_{0.7}GnP_{1.0}$. Herein, the C and N atoms which come from the soybean powders have finally combined with W atom to form α-W_2C, δ-WC and WN (tungsten nitride) NPs which is confirmed via XRD patterns (Fig. 7a1). The crystal facets of α-W_2C, δ-WC and WN can be further explored by comparing the XRD patterns with the standard JCPDS. As shown in TEM (Fig. 7a2) and HRTEM (Fig. 7a3) images, the GnP as the conductive support is decorated by α-W_2C, δ-WC and WN nanoclusters with a size range from 5 nm to 20 nm. Notably, α-W_2C and δ-WC contribute to the catalytic activity, while WN is the catalysis stabilizer. And the graphene was a metal-like connector and carrier to favor the charge transfer between the catalyst particles and the electrode to enhance the electrocatalytic activity. Through the investigation in HER, the $WSoy_{0.7}GnP_{1.0}$ demonstrated an overpotential of 105 mV at the current density of 10 mA cm^{-2} in 0.1 M $HClO_4$. The Tafel slope is 36 mV dec^{-1} which is approaching to the commercial Pt/C (31 mV dec^{-1}).

Tungsten oxide (WO_3)-based materials have the advantages of enhanced reaction kinetics, low cost, good catalytic stability, etc. and have become a considerable candidate for OER/HER electrocatalyst in recent years [110,111]. Furthermore, the high specific surface area and conductivity of biomass activated carbon (B-AC) make people have great interest in compounding it with WO_3 to produce high-performance AC-

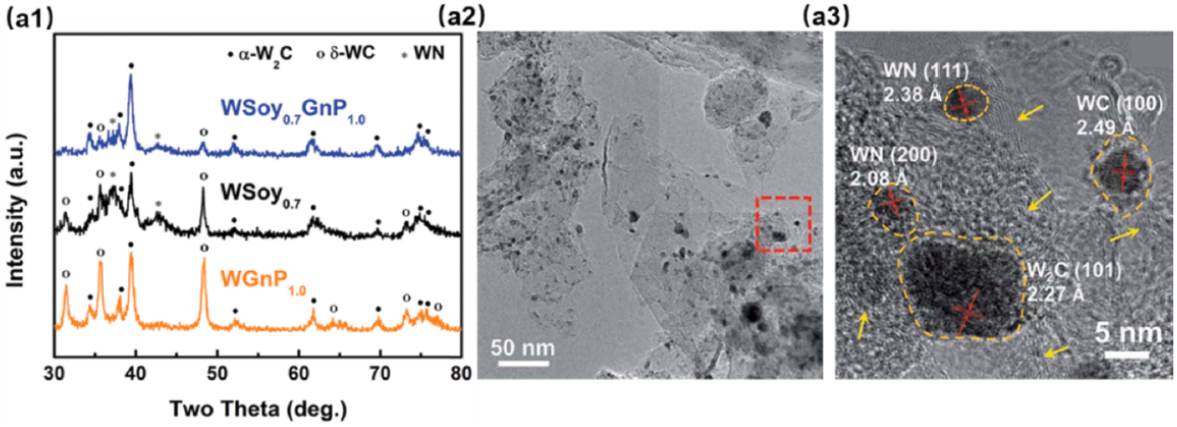

Fig. 7. **(a1)** XRD patterns of the $WSoy_{0.7}GnP_{1.0}$, $WSoy_{0.7}$ and $WGnP_{1.0}$ electrocatalysts, **(a2)** TEM image of the $WSoy_{0.7}GnP_{1.0}$, **(a3)** HRTEM image of the enlarged area in the red box in **(a2)**. Adapted with permission [56]. Copyright 2015, Royal Society of Chemistry. (For interpretation of the references to colour in this figure legend, the reader is referred to the web version of this article.)

WO_3 composite [112,113]. Lee's group designed a B-AC-anchored WO_3 Nanoflakes (WO_3/B-AC) through a simple sonochemical reaction [114]. The B-AC was firstly prepared from the neem leaves (Azadirachta Indica) via two-step thermal treatment. Then, the WO_3/B-AC was obtained by mixing B-AC and WO_3 nanopowders in DI water after 1 h of ultrasound. The WO_3/B-AC showed an outstanding electrocatalytic activity for HER in 1.0 M KOH compared with the pristine WO_3 nanoflakes. It required 360 mV to drive the current density to 10 mA cm^{-2}, while the value of WO_3 nanoflakes is 440 mV. Besides, the Tafel slope of the WO_3/B-AC is also lower than that of pristine WO_3 nanoflakes (14 mV dec^{-1} vs. 27 mV dec^{-1}). The better electrical conductivity of the WO_3/B-AC is attributed to the fact that WO_3 is encapsulated with highly conductive B-AC. Furthermore, the value of I_D/I_G is clearly increased after WO_3 nanoflakes loading on the B-AC nanosheets (0.71 vs. 0.90). indicating that the decoration of WO_3 nanoflakes will also promote the formation of defects.

The biomass-based carbon decorated with W-based compounds exhibited the excellent catalytic performance for HER. The biomass can not only supply the carbon skeleton to support catalysts, but also act as the C and N source to form metal compounds with W. The non-metal element (P, S, et al.) of biomass performs as the reactant with metal to produce the metal compounds. It is necessary to specify the reaction process for promoting the hybrid efficiency among the non-metal elements and metals.

4.2. Cobalt (Co)

The oxide [115], sulfide [116], phosphide [117] of Co have been extensively investigated as promising catalyst for HER. Moreover, under the protection of carbon support, the catalyst will show more stable

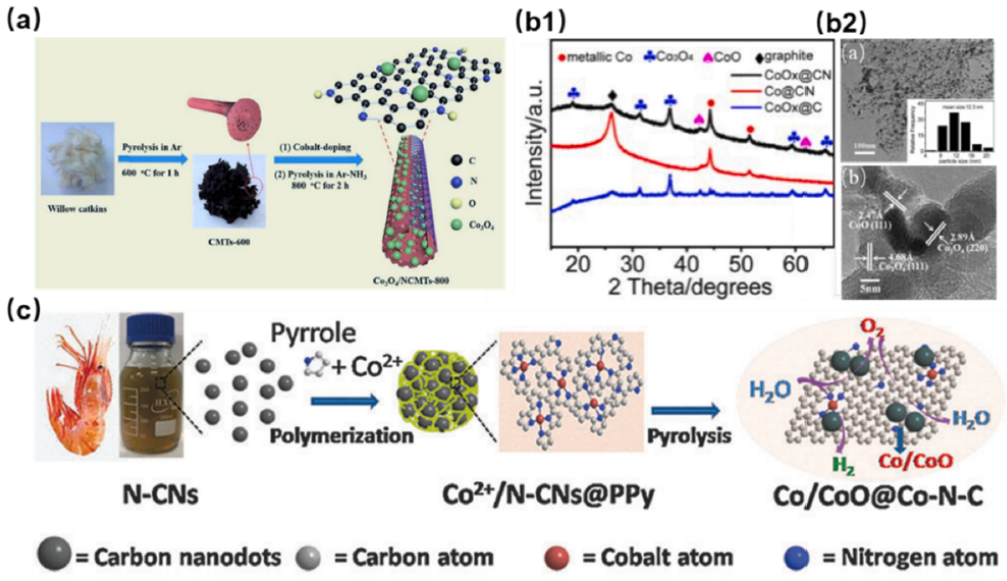

Fig. 8. **(a)** Schematic of the synthesis process for the Co_3O_4/NCMTs-800. Adapted with permission [122]. Copyright 2019, Elsevier. **(b1)** XRD patterns of CoOx@CN, Co@CN and CoOx@C, **(b2a)** SEM and **(b2b)** TEM images of CoOx@CN, the inset picture of **(b2b)** showing the corresponding particle-size distribution histogram. Adapted with permission [57]. Copyright 2015, American Chemical Society. **(c)** Schematic illustration of the synthesis of Co/CoO@Co–N-C. Adapted with permission [121]. Copyright 2016, Royal Society of Chemistry.

electrocatalytic activity [23,118]. Due to its superior performances such as high conductivity and specific surface area, widely available and cheap, biomass-derived carbon material is an ideal choice to be the carbon substrate.

The Co-based oxides and N-doped carbon matrices can synergistically improve the catalytic activities and it is promising tri-functional electrocatalysts for ORR, OER and HER [119]. As illustrated in Fig. 8a, Wang et al. prepared Co_3O_4/N-doped hollow hierarchical porous carbon microtubes by taking advantages of the natural morphology structure of micron grade tube in willow catkins [120]. The overpotential at 10 mA cm^{-2} is 210 mV when taking the HER experiment in 1.0 M KOH. Furthermore, Wang's group was surprised to find that the existence of multivalence Co will significantly enhance the electroactivity of the catalyst [57]. They designed a hybrid catalyst (CoOx@CN) consisted of Co/Co oxide (Co^0, CoO, Co_3O_4) and N-doped carbon via a one-pot thermal treatment method with the raw material of Melamine, $Co(NO_3)_2{\cdot}6H_2O$ and D(+)-glucosamine hydrochloride. The multivalence Co has been proved by X-ray diffraction (XRD) test in Fig. 8b1. As shown in TEM images in Fig. 8b2(a), the Co nanoparticles are homogeneously dispersed on the carbon matrix with a mean size of 12.3 nm. The lattice fringe spaces revealed in HRTEM images (Fig. 8b2 (b)) have further confirmed the existence of multivalence Co. The stability of the hybrid catalysts has been promoted with the metallic Co embedded on the carbon frameworks [27]. Through the HER experiment in 1.0 M KOH, it needed 232 mV to drive the current density to 10 mA cm^{-2}, and the Tafel slope is 115 mV dec^{-1}. It is believed that the existence of multivalence Co will significantly enhance the electroactivity of the CoOx@CN. Therefore, multivalent Co composites such as Co/CoO decorated biomass-derived carbon support have been studied by several groups [121,122]. With utilization of the natural abundant raw material such as shrimp-shell and holly leaves, the N-doped carbon support was obtained. Afterwards, the Co/CoO loaded on the N-doped carbon support can be synthetized through further polymerization and pyrolysis.

As depicted in Fig. 8c, the N-doped carbon nanodots (N-CNs) was obtained via hydrothermal process by Zhang et al. [121] By further polymerization and pyrolysis, the Co/CoO loading on the N-doped carbon support (Co/CoO@Co-N-C) can be synthetized. The as-obtained Co/CoO@Co-N-C shows a microporous structure with high surface area. The synergistic effect of Co, CoO and Co-N doping in a graphitic carbon lattice was proved to promote HER performance by creating catalytically active sites. By using the same biomass material, the Co_9S_8@NPC was fabricated through one-step molten-salt calcination method [123]. Elemental mapping demonstrates that the Co and S were homogeneously overlaid and P is uniformly dispersed on the entire carbon structure. It has been confirmed that Co_9S_8 and the dopant of P are active species that can provide more catalytic sites [124,125]. Hence, the Co_9S_8@NCP exhibited better electrocatalytic activity for HER compared with NC and Co_9S_8@NC in 1.0 M KOH.

The P dopant can capture electron from metal atoms for its higher electronegativity. The negatively charged P atoms acted as effective local sites to trap the positively charged protons from the electrolyte during HER process. Besides, phosphides possess better corrosion resistance in acid media to exhibit robust durable catalytic activity. Due to the significant effect of P doping on enhancing HER performance, the phosphides of Co are another attractive solution for HER catalysis. Using biomass macromolecule sodium alginate or campanulaceae leaves as precursors, CoP-modified N, P co-doped biomass carbon hybrid catalyst was prepared through several works [126–128], while the sources of P in these works mainly originated from the chemical reagent. It is more economical and more environmentally friendly to use biomass with natural N/P content as a template. Since P is the main nutrient element of yeast, it can be converted into P self-doped carbon matrix. Therefore, Hu's group designed a carbon architecture through hydrogen thermal and high-temperature treatment using yeast as biomass source [58]. With the in-situ phosphidation of Co during the high-temperature treatment, the metal phosphide (Co_2P) was highly dispersed on the surface of obtained porous carbon sphere. (Fig. 9a1) The porous and open structure, abundant surface functional groups, as well as the inert environment ensuring by the high-temperature carbonization would greatly contribute to the anchoring of Co species. Through the HER test in 0.5 M H_2SO_4, the Co_2P-C exhibited an outstanding performance as shown in Fig. 9a2 and a3, the overpotential to drive the current density to 10 mA cm^{-2} is 96 mV. The Tafel slope is 34 mV dec^{-1}, which is smaller than 20% Pt/C (68 mV dec^{-1}). The value of C_{dl} is high of 126.27 mF cm^{-2} which indicates the rich active sites on the surface of Co_2P-C. Zhou's group [50] reported that N/P co-doped carbon spheres decorated by Co and Co/P (Co-CoP@NPC) can maintain the sphere morphology of saccharomycete cells. The hollow Co-CoP@NPC spheres with size of ~ 1.6 μm dispersed on the reduction graphene oxide (RGO) exhibited high activity for catalytic HER. Similarly, Li's group synthesized a porous N-doped carbon material decorated with Co_2P (Co_2P/NC), and the dopant of N and P is from the pristine spirulina (Fig. 9b) [129]. Notably, the electrocatalytic activity for HER of Co_2P/NC was investigated in universal-pH range and exhibited a comparable activity with 20% Pt/C.

Various compounds of Co as the HER electrocatalysts generally possessed great activity. The nonmetallic element of biomass such as O, P, N can hybrid with Co to form the CoO_X, CoP or the structure of Co-N-C, which were mainly the active sites for catalytic HER. Especially, the mild conversion such hydrothermal and direct calcination was used to retain the original structural of biomass. It is serious to maximize the utilization of biomass characteristics for the preparation of high-performance carbon materials.

4.3. Molybdenum (Mo)

Mo-based compounds have attracted extensive attention in catalytic HER such as the carbide [130,131], sulfide [16,132], oxide [133,134], of Mo, etc. Among them, Molybdenum carbide (Mo_2C) has been anticipated as a promising electrocatalyst for HER due to its similar electronic properties to Pt-group metals [130,135,136]. Hence, there are extensive efforts devoted to investigating the HER performance of Mo_2C supported on the biomass-derived carbon. Mu's group demonstrated a facile solid-state reaction to prepare a Mo_2C quantum dot embedded N-doped graphitic carbon layer (Mo_2C QD/NGCL) [137]. The N-doped graphitic carbon layer (NGCL) was derived from the biomass extract, chitosan. The as-formed Mo_2C was proved by comparing the characteristic peaks with the standard card of JCPDS No. 15–0457. With the decorating of Mo_2C quantum dot, the value of the I_D/I_G increased from 1.02 to 1.05, suggesting the more defects in Mo_2C QD/NGCL compared with the NGCL. The obtained Mo_2C QD/NGC exhibited remarkable HER electrocatalytic activity and durability at a wide range of pH value. The Pt-like electronic configuration of Mo_2C endow its with active adsorption of hydrogen. The hydrogen desorption of Mo_2C was more favorable after coupling with carbon because the d-band of Mo would downshift and transfer the charge from Mo to C, which possessed more optimal Mo-H bong strength.

The carbon matrix doped with heteroatoms (S and N) have been confirmed for boosting the activity for Mo_2C to catalytic HER. The dopants and their adjacent atoms provided additional active sites. Moreover, the S/N atoms doping in the carbon lattice could regulate the d-orbitals of Mo_2C, tune the Fermi level [6]. As an biomass containing S elements, cellulose nanocrystals (CNC) have been used as the precursor to synthetize the carbon support for Mo_2C (Mo_2C@S-CA) [138]. The Mo_2C with size of 3 ~ 6 nm loading on the homogenous carbon nanorods (5 ~ 10 nm) was reveled via FESEM and TEM. Especially, the S containing group in CNC will promote the surface functionalization and create the self-doping of S to facilitate the exposure of active sites [138–141]. The Mo_2C@S-CA exhibited an excellent HER performance with the overpotential of 176 mV at 10 mA cm^{-2}, along with a small Tafel slope of 66.1 mV dec^{-1}, the enhanced catalytic activity can be attributed to the strong interaction between Mo_2C@S-CA networks and

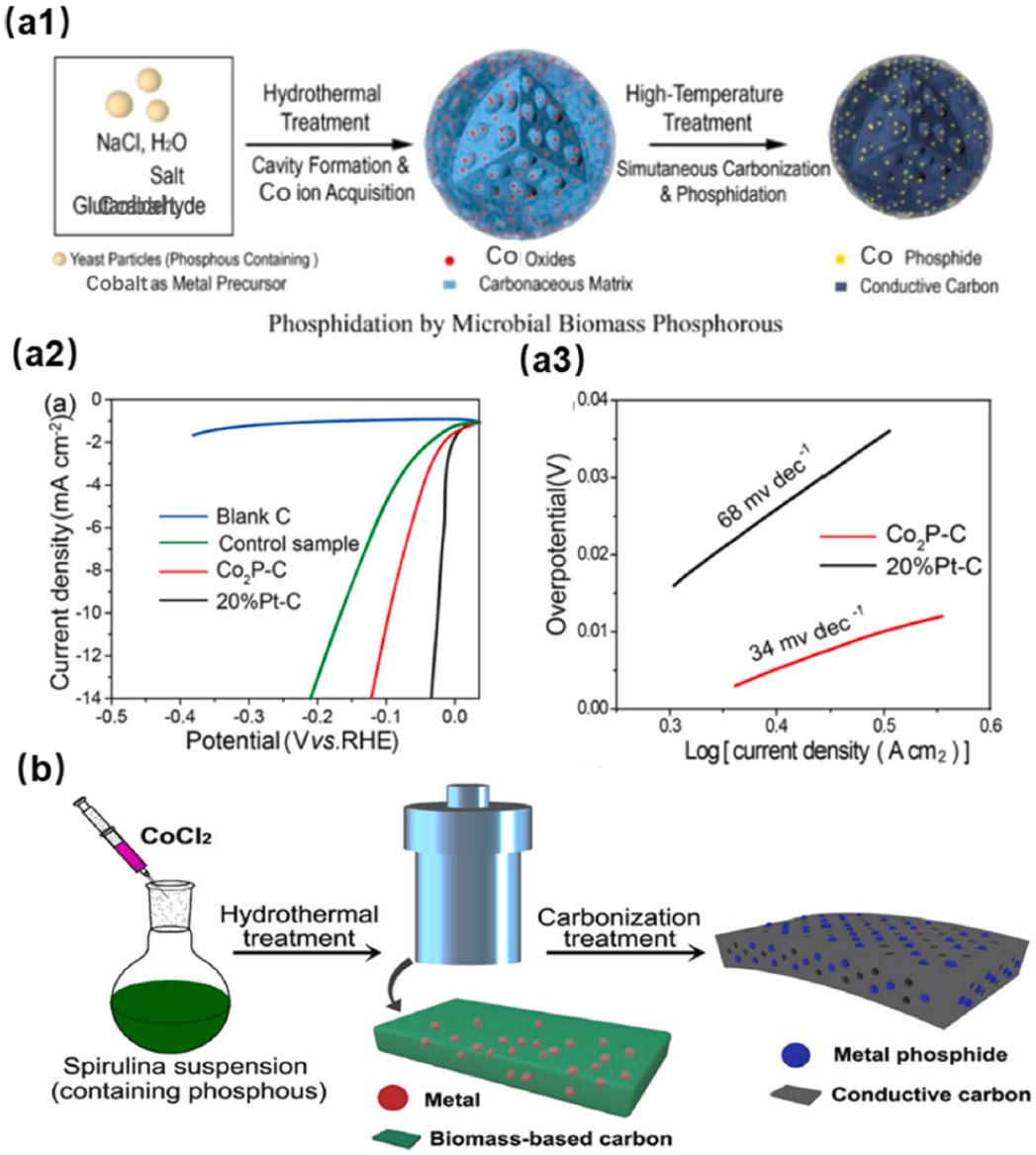

Fig. 9. **(a1)** Schematic illustration of the synthesis of Co_2P-C, **(a2)** Polarization curves of three different samples, including Co_2P-C, blank C, control sample, and 20 wt% Pt/C (tested in 0.5 M H_2SO_4 at a scan rate of 5 mV s^{-1}), **(a3)** Tafel plots of both Co_2P-C and 20 wt% Pt/C. Adapted with permission [58]. Copyright 2017, American Chemical Society. **(b)** Schematic illustration of the formation of Co_2P/NC. Adapted with permission [129]. Copyright 2019, Wiley.

S atom [138,142].

The bacterial cellulose can be produced via the microbial fermentation process which can be another ideal biomass precursor to prepare heteroatom-doped carbon nanofiber networks (N-CNFs) [143–145]. Wu and co-workers synthesized the ultrafine Mo_2C nanoparticles (<5 nm) embedded within N-CNFs (Mo_2C@N-CNFs) via the process of impregnation, freeze-drying and pyrolysis [54]. The HER performance was tested in a wide range of pH value, and the Mo_2C@N-CNFs showed a good activity in 1.0 M KOH with an overpotential of 168 mV at 10 mA cm^{-2} and a quite small Tafel slope of 47.1 mV dec^{-1}. Meanwhile, the Mo_2C@N-CNFs exhibited a better HER performance than CNFs, N-CNFs and commercial Mo_2C in acid electrolyte result from the synergistic effects between Mo_2C and N-CNF which is consistent with DFT study. By comparing the ΔG_{H^*} of Mo_2C@N-CNFs and Mo_2C@CNFs, the dopant of N was proven to play a critical role in enhancing the electrocatalytic activity.

Unlike biomass extracts, intrinsic biomass has more organic components (cellulose, lignin, etc.), which makes it possible to turn into various carbon matrix such as carbon sheet, carbon sphere etc. [55,146–148]. Through one-step solid reaction method, Mu et al. prepared the Mo_2C loaded on the porous graphitized carbon flake (Mo_2C/C) with using the cornstalks as the carbon sources [55]. The as-prepared Mo_2C/C exhibited a superior HER performance with overpotential of 114 mV to drive the current density to 10 mA cm^{-2} and a small Tafel slope of 52 mV dec^{-1} in acid electrolytes.

Thanks to the red jujube is full of organic matters, it will be converted into heteroatom dopants [149]. Chen's group fabricated Mo_2C decorated on the N and P co-doped porous microspheres (NP-Mo_2C/PCMS) via hydrothermal and following annealing treatment [146]. The size of microsphere is about 1 μm. The as-prepared NP-Mo_2C/PCMS exhibited

extraordinary electrocatalytic activity in the acid and alkaline electrolytes toward HER. Especially in alkaline solution, the overpotential is lower of 80 mV at 10 mA cm^{-2}, as well as a smaller Tafel slope of 46 mV dec^{-1}.

The S contained in sunflower seeds can produce S self-doped carbon matrix. Therefore, Mo_2C supported on N and S co-doped carbon matrix (Mo_2C@SNC) which is derived from sunflower seeds has been designed through one-step calcination reaction by An et al. (Fig. 10a1) [147]. The diameter of Mo_2C NPs ranges from 6 to 8 nm is shown in Fig. 10a2. According to the JCPDS card (No. 35–0787), the characteristic peaks in XRD patterns was confirmed to be the crystal facets of (100), (002), (101), (102), (110), (103), and (112) planes of β-Mo_2C. The as-synthesized Mo_2C@C showed a better electrocatalytic activity in 1.0 M KOH. The overpotential at 10 mA cm^{-2} is 60 mV and the Tafel slope is 71 mV dec^{-1}. With the application of similar synthesized strategy as reported by Yan et al., the porous β-Mo_2C nanoparticle clusters supported on carbon matrix (Mo_2C@C) derived from the walnut shell powders and ammonium heptamolybdate were obtained (Fig. 10b) [148]. The Mo_2C@C showed an excellent HER performance in 0.5 M H_2SO_4.

Dasog'group prepared a spiky-like Mo_2C with the birch tree derived carbon as the carbon source via a scalable solid-state magnesiothermic reduction reaction (Fig. 10c) [150]. The as-prepared Mo_2C appeared a great electrocatalytic activity without the carbon support in 0.5 M H_2SO_4. To drive the current density to 10 mA cm^{-2} and 100 mA cm^{-2}, the overpotential is as low as 35 mV and 60 mV, respectively. Furthermore, during the HER process, the hydrogen bubble was generated continuously for about 100 h which suggested a long-term stability.

Due to the low cost high-chemical stability and good catalytic performance towards HER, MoS_2 is the most widely researched TM dichalcogenides as the electrocatalytic for HER in recent years [151,152]. However, due to the low conductivity of MoS_2, the working efficiency of the single-component system is not high. Therefore, it is compounded with conductive materials such as carbon and can be effectively used for numerous applications. Several works of the research team have proved that the composite of MoS_2 and carbon-based materials can improve the electrochemical activity of the materials (for supercapacitors and HER) [153,154]. Selvakumar's group prepared the nanocomposites consisted of MoS_2 and the defective activated carbon (DAC/MoS_2) through simple grinding method [155]. Specifically, the 2D MoS_2 layers was synthesized by using the same method introduced in previous work with slight adjustment in reaction parameters [156]. Meanwhile, the activated carbon was produced from diospyros melanoxylon leaves via two-step thermal-treatment. Followed by hydrothermal N doping and high-temperature treatment, the DAC was obtained based on AC. The as-prepared DAC/MoS_2 exhibited an onset potential of 90 mV for HER, and the value of Tafel plot is 84 mV dec^{-1} which mainly attributed to the decoration of MoS_2.

The DAC/MoS_2 prepared via facile grinding could not make full use of the excellent electrocatalytic activity of MoS_2 for HER. Therefore, the method of assembling MoS_2 and biomass-derived carbon into hybrid catalyst needs to be future developed. Through the facile hydrothermal and followed by annealing, the amorphous carbon supported MoS_2 (MoS_2/AC) was fabricated for the first time by using the glucose as the source of C element [157]. The MoS_2 nanosheets vertically grew on the carbon nanosphere have assisted in the exposing of catalytic active sites,

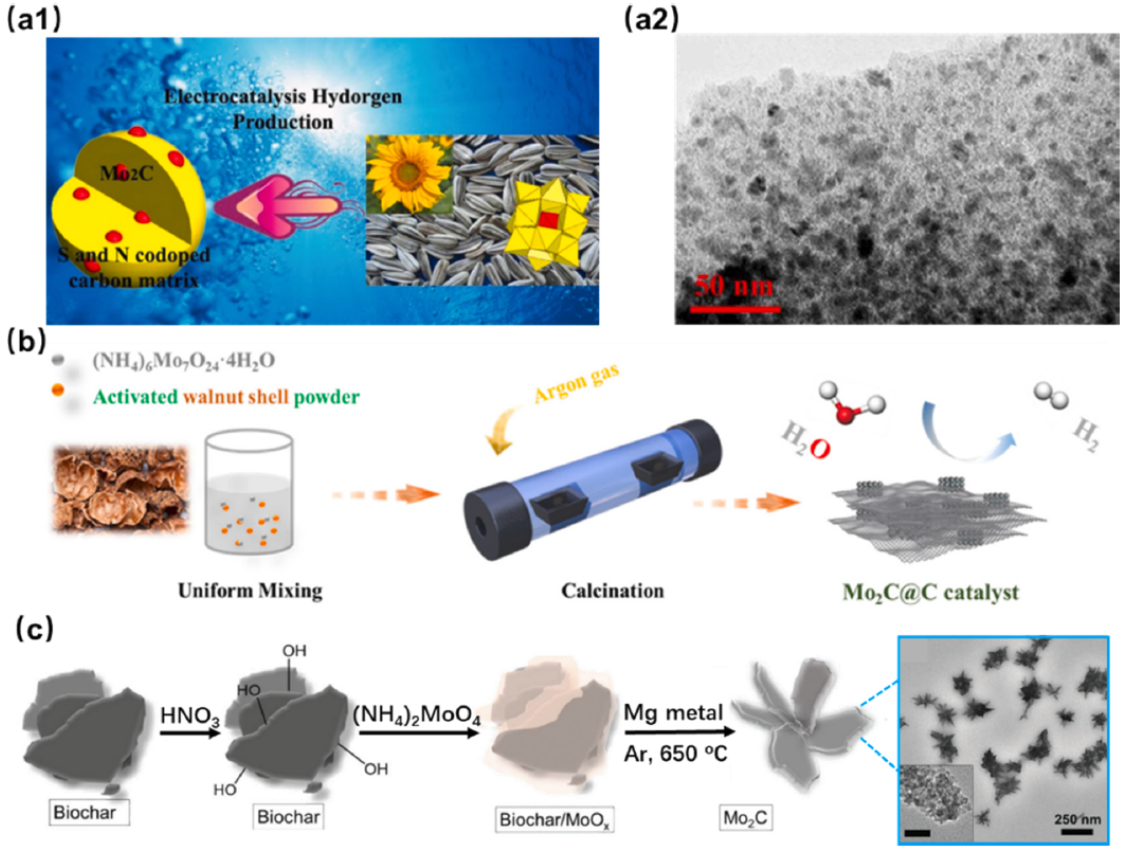

Fig. 10. **(a1)** Schematic illustration of the synthesis of Mo_2C@C nanocomposite, **(a2)** TEM image of Mo_2C@SNC. Adapted with permission [147]. Copyright 2017, American Chemical Society. **(b)** Preparation process for Mo_2C@C catalysts. Adapted with permission [148]. Copyright 2020, Elsevier. **(c)** Schematic illustration of the formation of Mo_2C nanostructures. Adapted with permission [150]. Copyright 2018, Wiley.

while the carbon support will enhance the conductivity of hybrid catalyst. The existence of hexagonal MoS_2 of (1 0 0) and (0 0 2) planes was proved by HRTEM and XRD tests.

The reassembled hybrid catalysts exhibited enhanced catalytic performance for HER in 0.5 M H_2SO_4. The onset potential is 80 mV, while the value of pure MoS_2 and commercial bulk MoS_2 is 180 mV and 170 mV respectively. The Tafel slope is 40 mV dec^{-1} which is approaching to 20% Pt/C. Through the similar synthesize method of hydrothermal, Qiao and co-workers demonstrated a simple approach of hydrothermal to prepare a biomass carbon tube matrix (BCTM) with MoS_2 loading (MoS_2/BCTM) [158]. Before that, the BCTM have been manufactured through freeze drying and pyrolysis process. The well dispersed MoS_2 nanosheets have greatly promoted the pore creation, while the carbon support of BCTM can significantly enhance the conductivity of MoS_2 nanosheets. Compared with pure BCTM and MoS_2 catalyst, the MoS_2/BCTM showed an excellent electrocatalytic activity toward HER due to the synergistic effects between the MoS_2 nanosheet and BCTM. In 0.5 M H_2SO_4, the overpotential at 10 mA cm^{-2} is 176 mV, and the Tafel slope is 51 mV dec^{-1}.

MoP has been utilized in a variety of hydroprocessing reaction and proven to show a higher catalytic activity than MoC and MoN [159–163]. Hence, MoP may be a potential electrocatalyst for HER. Through a facile synthesis method of solid-state reaction, the MoP nanosheets decorated on carbon flake (MoP/CF) was prepared using ammonium heptamolybdate tetrahydrate ($(NH_4)_6Mo_7O_{24}{\cdot}4H_2O$), sodium dihydrogen phosphate dihydrate ($NaH_2PO_4{\cdot}2H_2O$) and sodium alginate [164]. The as-prepared MoP/CF was investigated in both acid and neutral electrolyte and presented good electrocatalytic activity and durability in both two electrolytes.

Binary phase of Mo-based compounds has been intensively studied due to its extraordinary electronic and mass-transfer properties [165–167]. The synergistic effect between β-Mo_2C and γ-Mo_2N in promoting HER catalytic activity have been demonstrated by Chen et al (Fig. 11a) [168]. Such hybrid catalyst (Mo_1Soy) showed an excellent electrocatalytic activity for HER in 0.1 M perchloric acid ($HClO_4$) with a low overpotential of 177 mV at 10 mA cm^{-2}. Notably, a robust durability for more than 500 h operation in the acid electrolyte was obtained for the Mo_1Soy. In addition, the HER performance of the Mo_1Soy can rival to the commercial Pt/C when the Mo_1Soy was loaded on graphene sheets. Since the Mo_1Soy/RGO promotes the HER electrocatalytic activity through the synergistic effect between β-Mo_2C and γ-Mo_2N, the Mo_2C/Mo_2N decorated biomass template was developed via a high-temperature solid-state reaction process by Vivek's group (Fig. 11b1) [169]. The biomass template chosen in this report is cotton which is full of natural fibrils. The use of templates not only promotes the charge transfer through the catalyst interface but also provides carbon support during the reaction. The crystalline Mo_2C/Mo_2N was the hexagonal β-Mo_2C and cubic γ-Mo_2N via PXRD. As shown in element mapping in Fig. 11b2, the Mo_2C/Mo_2N with diameters range from 10 ~ 12 nm was uniformly dispersed on the fibrils template. Through the HER tests in 0.5 M H_2SO_4, the onset potential is 110 mV, along with an overpotential of 176 mV at 10 mA cm^{-2}, while the Tafel slope is 64 mV dec^{-1}. (Fig. 11b3) This research will provide exciting insights for the growth of biphasic Mo derivative catalysts on natural biomass matrix. It will also introduce a new system for the basic study of nanohybrids and apply it to realistic energy conversion system.

Most of Mo-based compounds (MoP and MoS_2) was prepared by hydrothermal with using other chemical reagents as the source of nonmetallic. It was attractive to obtain Mo-based phosphide and sulfide through in-situ growth protocol, because the P and S is rich in most of biomass sources. In addition, nonmetal elements of biomass could be introduced into biomass-derived carbon as dopants, because the carbon doped with heteroatoms would increase the active sites and optimize the Mo-H bond energy to moderate value.

4.4. Nickel/Iron (Ni/Fe)

Metallic Ni is a promising electrocatalytic for HER in alkaline due to its minimum ΔG_{H^*} value and a maximum HER exchange current density among various nonprecious metals [6]. The rich lignocellulose, protein and carotene in carrots make it to be a potential precursor [170]. Therefore, Van et al. reported an environment-friendly and facile route to prepare Ni NPs decorated on P-doped carbon materials [171]. The as-obtained Ni NPs was proved to be anchored on the carbon substrate as the Ni and nickel oxide (NiO) nanoparticles with a diameter of 15 ~ 50 nm via XRD and HRTEM. The PC-$Ni_{0.75}$ exhibited a Tafel slopes of 134.9 mV dec^{-1} and overpotentials of 297 mV to reach 10 mA cm^{-2} for HER. They found that the addition of Ni NPs has an important effect on the number of active sites of HER. It was known that Ni/NiO NPs were embedded on nitrogen-doped graphene displayed an excellent HER activity as reported in the work of Wang et al. [172]. Then, Van et al. immediately reported an inexpensive synthetic one-step synthetic route to prepare Ni/NiO NPs immobilized on nitrogen-doped activated carbon derived from cauliflower leaf (NiO_X-AC-500) [173]. The large specific surface area means large number of active sites and the abundant nitrogen functional groups in the biomass-derived activated carbon are beneficial to the close contact between Ni/NiO NPs and carbon skeleton. In the investigation in HER, the NiO_X-AC-500 needed 180 mV to reach

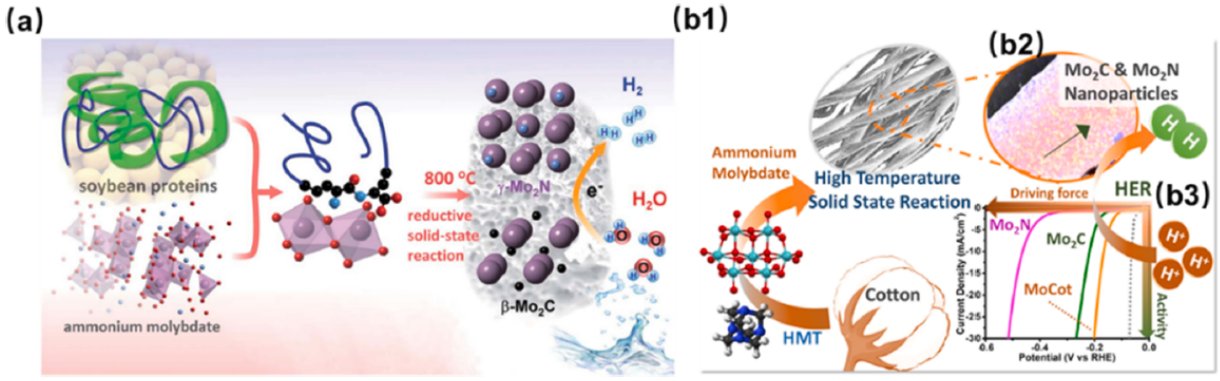

Fig. 11. **(a)** The synthesis from soybeans and ammonium molybdate of a solid catalyst suitable for electrochemical hydrogen production. A solid-state reaction between soybeans and the molybdate leads to their reductive carbonization and nitridation, so as to form β-Mo_2C and γ-Mo_2N crystals. Adapted with permission [161]. Copyright 2013, Royal Society of Chemistry. **(b1)** Illustrating the synthesis of the carbon supported Mo_2C/Mo_2N nanohybrid, **(b2)** HRTEM image shows the collective distribution of different elements (Mo, C, and N) on the fibril structure, **(b3)** Polarization curves (iR-corrected) of MoCot compared with the other electrode. Adapted with permission [169]. Copyright 2018, American Chemical Society.

10 mA cm^{-2} and demonstrated an excellent stability over 2000 CV cycles in 0.1 M KOH.

Thermal carbonization requires a low heat input, no high-cost metals and eco-friendly which is a facile technique compared with other physical or chemical treatments. Meanwhile, reducing the energy cost in the carbonization process is of great significance for large-scale production. Hence, Jiang et al. presented a Ni treatment method to anneal filter paper to graphitized carbon materials by reducing the carbonization temperature from 1500 °C to 800 °C as shown in Fig. 12a1 [174]. The onset potential of HER of NiP-800 shifted to −0.26 V and −0.17 V for activation of 4000 and 12,000 CV cycles respectively as depicted in Fig. 12a2. In the continuous CV activation process, Ni atoms can easily to find the most stable binding site structure, thereby making the newly grown Ni surface more organized and crystalline, thus efficiently improved the HER activity.

Wood possesses many aligned vertical channels, higher density and a dense structure, playing a vital role in the multiphase contact reaction process [175–177]. In addition, the wood surface with a large number of active sites provide a deep foundation for firmly grasping metals or their compounds [178]. Based on the above advantages of wood, Hu's group firstly reported a wood derived carbon framework embedded with N-doped, few-graphene-layer-encapsulated NiFe alloy NPs (CW-CNT@N-C-NiFe) via using rapid heat shock treatment [179]. The average size of N-C-NiFe was 22.5 nm detected by particle size analysis, which is 22.2 times smaller than N-C-NiFe nanoparticles prepared through conventional pyrolysis. The crystal NiFe was proved to Ni_3Fe alloy through XRD tests. The Ni_3Fe alloy anchored on the unique channel structure of N-doped graphene layer endowed the hybrid catalysts with a lowest $\triangle G_{H^*}$ value(-0.03 eV), which will leads more optimal H^+ absorption and electrocatalytic activity. The CW-CNT@N-C-NiFe thus showed a low overpotential (59 mV) at 10 mA cm^{-2} and low Tafel slope (52.8 mV dec^{-1}) in acid solution. It is of great significance to study the alkaline water electrolysis mechanism of wood skeleton in alkali solution which is widely used in industry. Therefore, Hui et al. developed a natural wood-based 3D framework loaded on an amorphous NiP alloy (NiP/Poplar wood) through a facile electroless plating method (Fig. 12b) [180]. The NiP/Poplar wood exhibited a prominent HER activity. It needed 83 mV to drive a current density of 10 mA cm^{-2}. In addition, it showed a small Tafel slope of 73.2 mV dec^{-1} in alkaline solution. This work provides a new pathway for the optimization of transition metal phosphides (TMPs) and natural multi-channel wood to obtain high HER electrocatalytic activity.

Phytic acid (Myoinositol 1, 2, 3, 4, 5, 6-hexakisphosphate, PA) is a green organic phosphate compound extracted from plant seeds. Six phosphate groups in PA can not only be used as P source, but also be easily crosslinked with metal precursors [45,181–183]. Thus, Pu et al. demonstrated a green method to fabricate FeP NPs encapsulated in NPC matrix (FeP NPs@NPC) by pyrolyzing self-assembled PA cross-linked metal complexes and melamine [184]. The FeP (111) nanoparticles with mean size of 160 nm was well loaded on the N, P doped carbon support. The synergistic effects between FeP and NPC layers leaded an excellent HER activity at all pH values. It needed 130, 386 and 214 mV in 0.5 M H_2SO_4, 1.0 M phosphate buffer solution (PBS) and 1.0 M KOH respectively to drive a current density of 10 mA cm^{-2}. In addition, the encapsulation by NPC effectively prevented the corrosion of FeP NPs, and exhibited almost unaffected catalytic activity after 10 h testing at all pH values. Therefore, this synthesis idea opens a door for the design and preparation of new low-cost TMPs-based electrocatalysts.

Biomass enriched in P-related components was another attractive protocol, leading to lead to in-situ phosphating of metals to form phosphides [58]. Li and co-workers [51] prepared the heterostructure Ni-Ni_3P embedded into N, P-doped carbon on graphene frameworks (Ni-NiP@NPC/rGO) by using the saccharomycete cells. The particles of Ni and Ni_3P with a size ~ 60.49 nm uniformly dispersed on the hollow carbon sphere of 1 ~ 1.6 μm. The Ni-NiP@NPC/rGO exhibited a small overpotential at 20 mA cm^{-2} of 113 mV, together with a Tafel slope of 57.93 mV dec^{-1}. The heterostructure Ni-Ni_3P leaded an optimal ΔG_{H^*} of −0.075 eV which could efficiently weaken the strong Ni-H bonding and promote the desorption process of H ions, thus yielding a faster HER kinetics.

P involved in biomass can be introduced into hybrid materials as heteroatoms [185]. The P-doped Fe_3N was encapsulated by N-doped carbon nanosheets grown on Fe foam substrate (P-Fe_3N@NC NSs/IF) gave excellent activity of electrocatalytic HER in 1.0 M KOH and durable

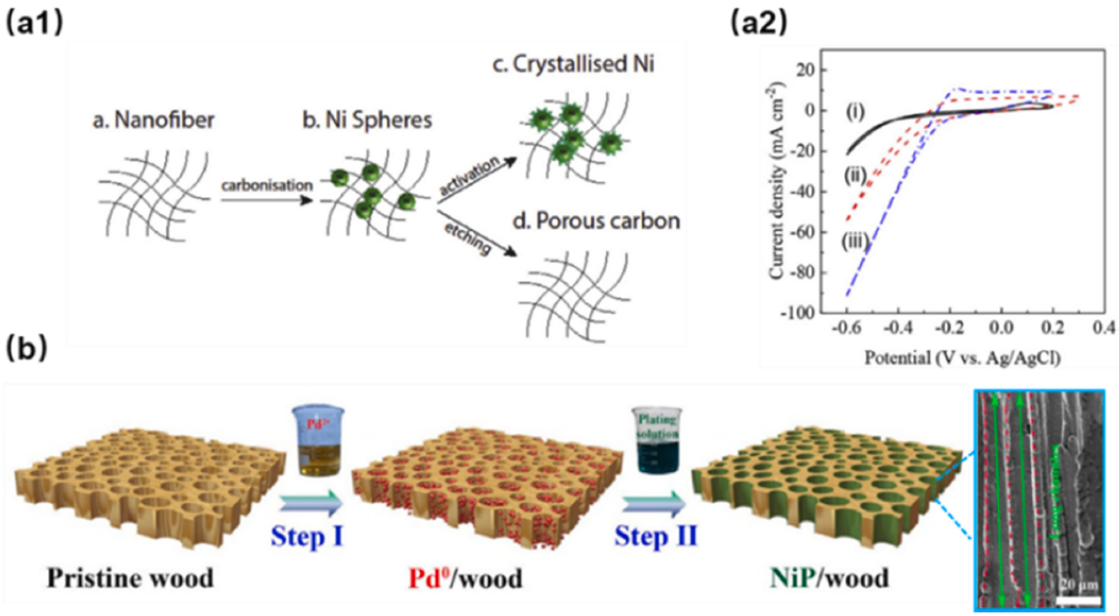

Fig. 12. **(a1)** Brief diagram of the synthesis of NiP-800, **(a2)** CVs in 0.5 M H_2SO_4 at NiFP-800 (i) before electrochemical activation, (ii) after 4000 cycles activation, (iii) after 12,000 cycles activation. Adapted with permission [174]. Copyright 2018, Elsevier. **(b)** Schematic representation of the preparation of NiP/wood. (Step I represent the activation process and Step II represent the plating process). Adapted with permission [180]. Copyright 2019, Elsevier.

stability. The dopants of P effectively regulated the electron density state which was proved by DFT results. And Fe sites of as-prepared Fe_3N NPs was the active centers which possessed high electrocatalytic for HER.

Ionic liquids (ILs) possess an adjustable hydrophilicity, ionic nature, high chemical stability, and good thermal stability [186,187]. It has been shown to maintain a uniform distribution during carbonization process [188–192]. Making use of the affinity of ILs, Liu et al. designed uniform Fe_3O_4 NPs decorated on willow catkins derived hollow carbon microtubes (Fe_3O_4/NCMTs-800(IL)) [193]. Here, as shown in Fig. 13a1, the ionic liquid (Fe-IL) controls the size of the Fe_3O_4 NPs, inducing uniform distribution of Fe_3O_4 NPs on hollow porous carbon microtubes. The Fe_3O_4/NCMTs-800(IL) afforded a small overpotential at 10 mA cm^{-2} for HER (170 mV) (Fig. 13a2).

Previous studies have shown in contrast to monometal-decorated carbon, synergistic benefits can be obtained by combining different monometals, and found that compared with other bimetals (i.e., FeCo, NiFe, FeMn, CoNi, MnCo, and NiMn) materials, the synergistic effect of NiFe contributes the most to catalysis [194–199]. Therefore, NiFe decorated, N, P and S tri-doped nanocarbon with oxygen-containing groups ($Ni_{0.25}Fe_{0.75}$-N, P, S) was reported by Wang et al. [200]. The synthesis process is illustrated in Fig. 14a, Alfalfa is rich in N, P and S, works as the sole carbon and heteroatom precursor. The Ni and Fe nanoparticles existed as both the metallic and alloy phase distributed on the surface of the carbon support. Take the HER experiment in 1.0 M KOH, the $Ni_{0.25}Fe_{0.75}$-N, P, S showed a prominent HER activity with a low overpotential of 250 mV at a current density of 10 mA cm^{-2} and a small Tafel slope of 84 mV dec^{-1}.

Electrolyzer coupled with photovoltaic modules to produce solar-powered hydrogen are a desirable sustainable energy conversion system. Therefore, Kumar et al. demonstrated a novel method to synthesize duckweed (DW) derived N, S-doped mesoporous carbon matrix supported bimetallic NiFe alloy nanoparticles as efficient earth-abundant electrocatalysts (NF-8-A) (Fig. 14b1) [201]. According to the XRD patterns, the TM existed in the NF-8A was only the phase of the face centered cubic Ni-Fe alloy. The NF-8-A required 215 mV at 10 mA cm^{-2} in 1.0 M KOH. The DW derived electrolyzer integrated with perovskite solar cell module can produce quite stable photocurrent of water decomposition (Fig. 14b2), and the conversion efficiency of solar-to-hydrogen (STH) is 9.7%, which provides an opportunity for its practical and expandable application.

The compounds of Ni or Fe were commonly the additives in the chemical activation process of biomass. The Ni and Fe were mainly to form the active sites for catalytic HER. Through the combination of the activation and decoration in one step, the Ni/Fe modified carbon material can be obtained. The synchronous activation-decoration is considered to be an economical and environmentally friendly method for the preparation of highly-efficient biomass-based HER catalyst.

4.5. Noble metal

Reducing the Pt content in the catalyst is another feasible strategy to decrease the cost of the electrocatalyst, which may promote industrial application of hydrogen production from water splitting. 20% Pt/C is the most used commercial electrocatalyst for HER, but the price is as high as about 130 dollar per 1 g. Kalyani et al. developed an activated carbon derived from turf grass and areca leaves as matrix for Pt [202,203]. It is remarkable that the loading amount of Pt is only 1% which will be more economical. The clean biomass precursor was firstly mixed with $ZnCl_2$ solution, and then the dehydrated mixture was calcined at 250 °C for 2 h to obtain the activated carbon. The Pt loaded on the activated carbon via water reduction reaction. Compared with the pure activated carbon, the electrocatalytic activity of the hybrid catalyst was enhanced by the decoration of trace Pt.

Ru have a moderate hydrogen bonding energy (about 65 kcal mol^{-1}) as a member of Pt-group metals, while the price of Ru is only 4% of Pt [6]. Ru can be used as an ideal alternative electrocatalyst for Pt, which has been received extensive attention in many reports [204–210]. The aggregation phenomenon during the HER process will seriously affect the stability of Ru-based catalyst. Studies have shown that designing a matrix loaded with Ru NPs is a promising strategy that can improve its durability by eliminating agglomeration [209,211]. Wang's group synthesized the Ru-doped Mo_2C embedded in N-doped carbon matrix (Mo_2C@Ru) (Fig. 15a1) [212]. The raw corns were firstly heated in a sealed container to obtain popcorn like previous reports [213,214]. The obtained popcorns were mixed with KOH to form "popcorn-hominy" solution. Then, the $(NH_4)_6Mo_7O_{24}{\cdot}4H_2O$ was throwed into the as-obtained solution and stirred for 6 h and the homogeneous solution was dehydrated via freeze-dried after adding the $RuCl_3$. Finally, the hybrid catalyst was prepared by an annealing the solid mixture. Through the annealing treatment, the popcorns derived carbon not only developed the carbon matrix, but also formed Mo_2C with Mo and the Ru^{3+} was reduced to Ru NPs [215]. Notably, Ru nanoparticles loading on the surface of Mo_2C with a loading amount of 7.6 wt%. The hybrid Mo_2C@Ru was uniformed dispersed on the carbon framework derived from popcorn with a size range from 3 to 8 nm. The crystal facets of Mo_2C (1 2 1) were confirmed via both XRD and HRTEM. As depicted in Fig. 15a2, through HER experiment in 0.5 M H_2SO_4, the Mo_2C@Ru exhibited an excellent performance with an overpotential of 24.6 mV and 66.5 mV to drive the current density to 10 mA cm^{-2} and 50 mA cm^{-2}, respectively.

Carbon quantum dots (CQDs) as a zero-dimensional material with extraordinary physicochemical properties attracted world-wide attentions in various photo-electrochemical fields [53,216–218]. As an excellent electron donors and acceptors, CQDs not only favor the electron and charge transport, it also protected the metal NPs without agglomeration to guarantee the stability of electrocatalysts. Ru-based NPs loaded on the biomass-based CQDs was an up-to-date concept for

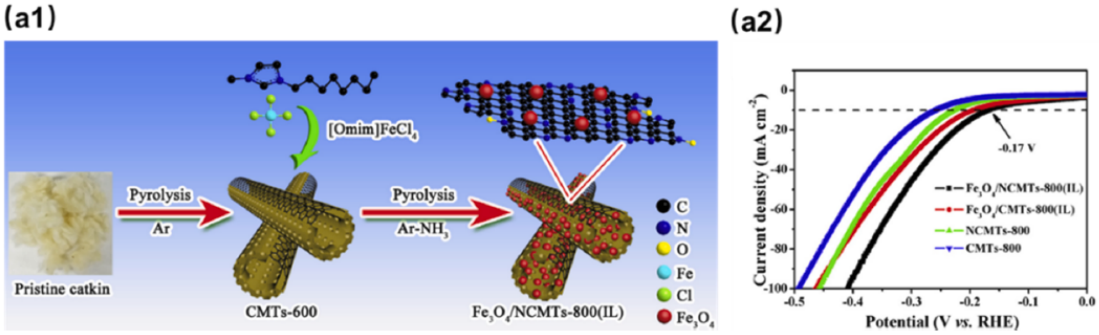

Fig. 13. **(a1)** Illustration of the preparation process of Fe_3O_4/NCMTs-800(IL), **(a2)** HER electrolysis polarization curves for Fe_3O_4/NCMTs-800(IL), Fe_3O_4/CMTs-800 (IL), NCMTs-800 and CMTs-800 in 1 M KOH solution. Adapted with permission [193]. Copyright 2019, Elsevier.

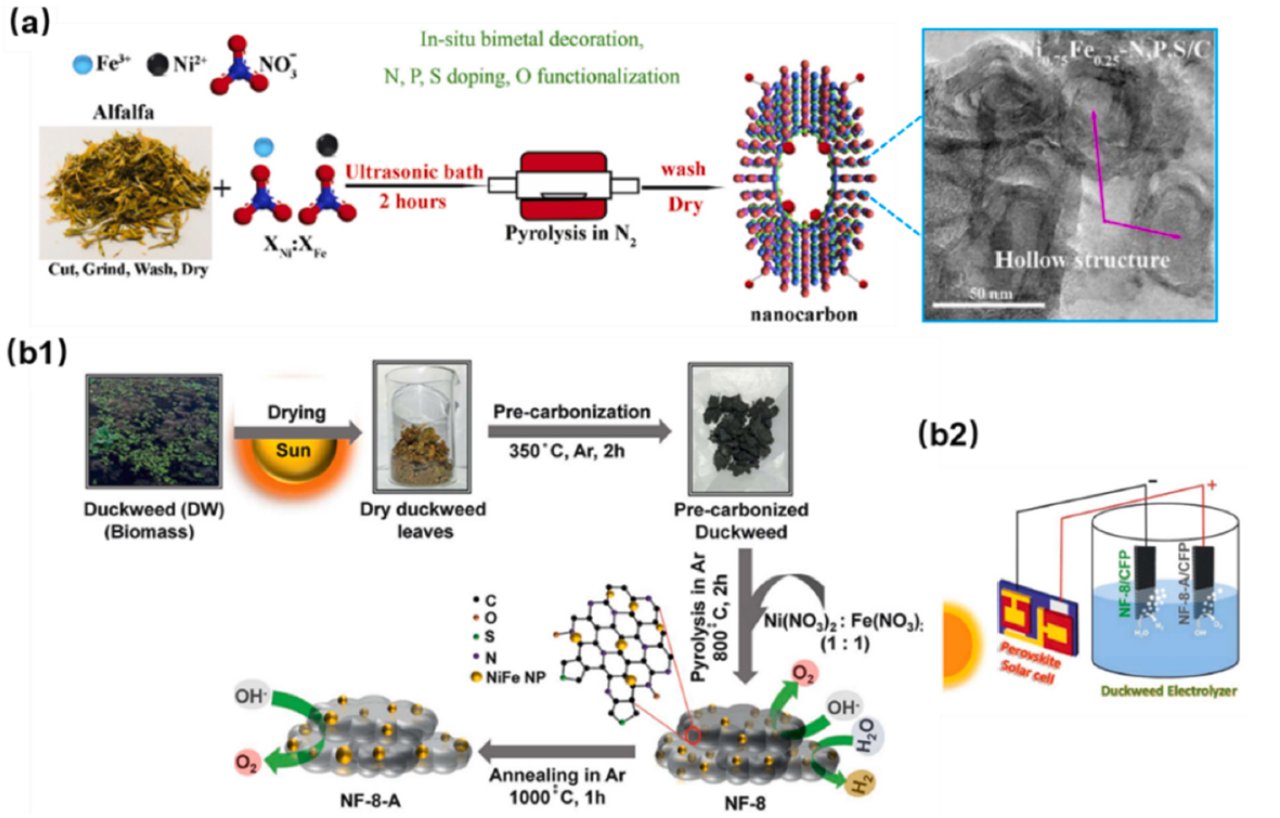

Fig. 14. **(a)** In-situ synthesis of NiFe-decorated, N, P, S tri-doped nanocarbon with rich O-containing groups and structural defects. Adapted with permission [200]. Copyright 2018, Elsevier. **(b1)** Schematic illustration of the synthetic process of NF-8 and NF-8-A by one-step conversion from pre-carbonized duckweed, **(b2)** Schematic illustration of the solar-energy-driven overall water splitting device with a perovskite solar cell. Adapted with permission [201]. Copyright 2019, Royal Society of Chemistry.

designing HER electrocatalyst [219–221]. With a lower mass concentration of Ru NPs of 3.78 wt%, Li and co-workers demonstrated a facile pyrolysis strategy to prepare the Ru NPs decorated carbon quantum dots (Ru@CQDs) [222]. As illustrated in Fig. 15b1, the CQDs was obtained firstly via hydrothermal treatment using the ginkgo leaves, followed by another hydrothermal process to mix the as-prepared CQDs with $RuCl_3$ to achieve a membranous structure. The Ru@CQDs480 was prepared by further annealing at 480 °C for 2 h. The hexagonal Ru NPs of were homogenously dispersed on the surface of the CQDs with an average size of 3.28 nm as shown in Fig. 15b2. Surprisingly, the Ru@CQDs480 exhibited an overpotential of 10 mV to afford the current density of 10 mA cm^{-2} without IR correction in 1.0 M KOH, which is 20 mV lower than that of 20% Pt/C. The synergic effect between Ru NPs core and CQDs greatly promote the electronic transfer through reducing the charger-transfer resistance (Rct-Ru@CQDs480 = 6.35 Ω vs. Rct-20% Pt/C = 11.08 Ω). Moreover, it is worth admirable that the cost of Ru@CQDs480 is only 0.80% of 20% Pt/C. Lu's group [223] presented the porphyra-CQDs-supported Ru NPs catalysts (Ru@CQDs800) to catalytic HER (Fig. 15c1). Compared to the hybrid material prepared by direct pyrolysis of Ru and porphyra/porphyra-based activated carbon, the CQDs is estimated to be better for the dispersion of Ru NPs (~2.21 nm) (Fig. 15c2). The overpotential for Ru@CQDs800 to drive the current density to 10 mA cm^{-2} was only 65 mV in 1.0 M KOH, as well as a small Tafel slope of 63 mV dec^{-1}. The loading amount of Ru was only 1.24 wt%. When the biomass-based CQDs was modified by Ru and Co NPs, the catalysts possessed a smaller overpotential than that of commercial Pt/C at 10 mA cm^{-2} [224].

In addition of Ru-based electrocatalysts, Palladium (Pd) have been loaded on the CQDs (n-Pd@NDCDs) to prepare HER electrocatalysts due to its moderate value of $\triangle G_{H^*}$ [225]. The CQDs with a size range from 1 to 9 nm was derived from the M. citrifolia fruit by hydrothermal process. The aqueous NH_3 was added in the hydrothermal process to introduce more N dopants into CQDs. The activated carbon derived from biomass was another support for Pd NPs [226]. Cardoso et.al [226] have prepared the activated carbon using vine shoots (Pd/VSAC) and grape stalks (Pd/GSAC) for the support of Pd NPs. For comparison, Vulcan XC72 carbon black was also used to synthesized carbon support for Pd NPs (Pd/Vulcan). Since the small specific surface area and no heteroatoms dopants of Vulcan-derived activated carbon, the Pd/Vulcan exhibited relatively poor HER behavior compared with Pd/VSAC and Pd/GSAC. Due to the better dispersion of Pd NPs, the Pd/VSAC showed a lower overpotential at 10 mA cm^{-2}. Therefore, compared with traditional carbon materials, it is feasible to make use of the advantages of biomass derived carbon materials as a metal carrier such as relatively large specific surface area and abundant heteroatoms to construct efficient hydrogen evolution catalyst.

Rhodium (Rh) is one of alternative for Pt electrocatalysts toward HER which have been explored extensively [227,228]. The relatively high loading amount and low activity seriously limited the application of Rh-based electrocatalyst. It is an appealing protocol to using the biomass-derived carbon materials as the support for Rh NPs to enhance the activity [229,230]. Liu et. al [229] have prepared Rh decorated N/S doped carbon (0.5Rh-GS1000) by using the biomolecule precursor (guanine). The N/S doped carbon sheets with high surface area benefited the homogenous dispersion of Rh NPs, thus greatly improved the activity of 0.5Rh-GS1000. Since the carbon support is worth to the dispersion of Rh NPs and protect it away from aggregation, ultrasmall Rh NPs decorated on N doped carbon nanotubes with encapsulated Ni

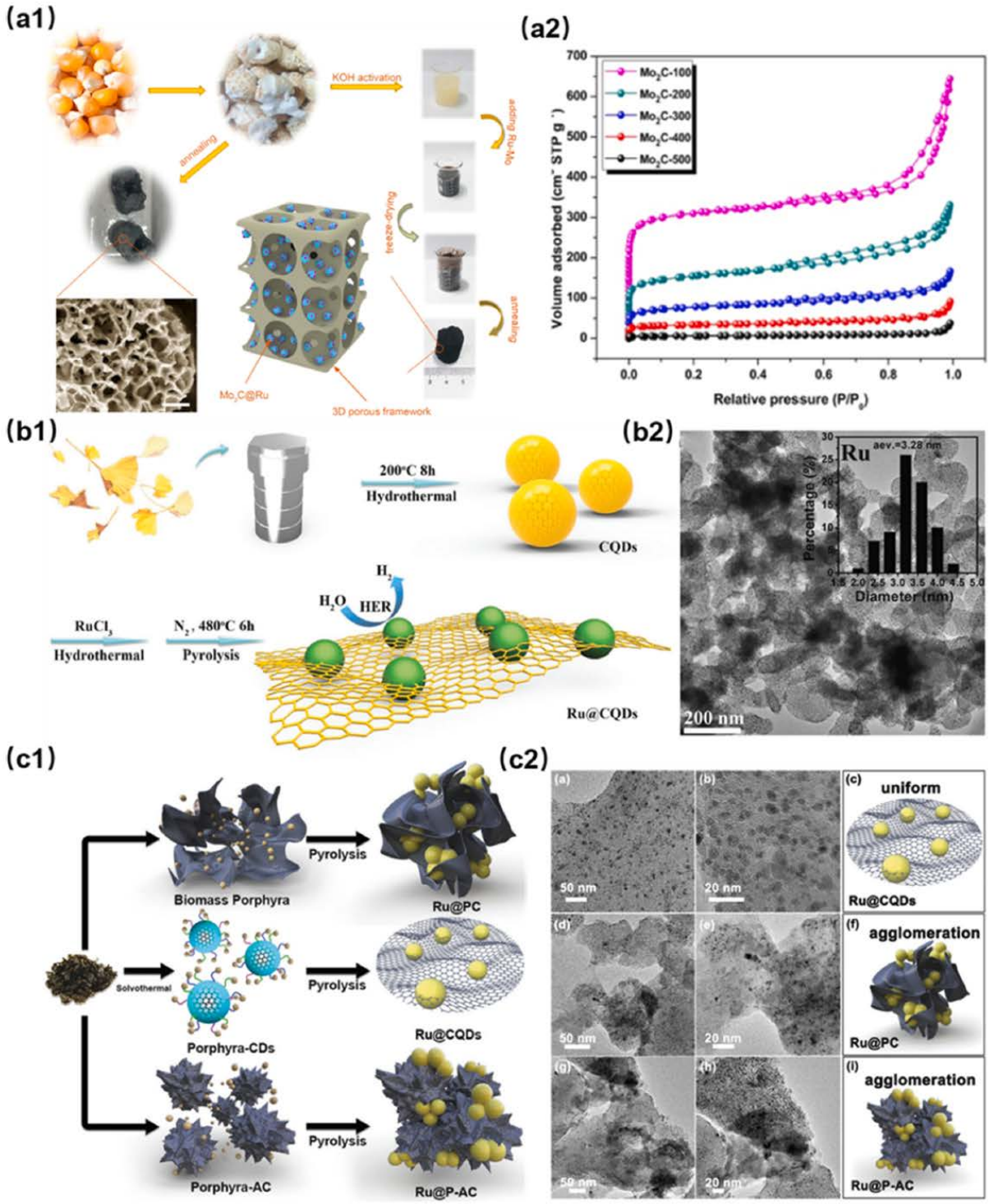

Fig. 15. **(a1)** Illustration of the preparation process of Mo_2C@Ru embedded in the 3D porous popcorn-derived carbon matrix, **(a2)** Polarization curves of Mo_2C@Ru, Mo_2C-300, Ru, commercial Ru/C, and commercial Pt/C. Adapted with permission [212]. Copyright 2018, American Chemical Society. **(b1)** Schematic illustration of the synthesis of the Ru@CQDs480 electrocatalyst, **(b2)** TEM image of as synthesized Ru@CQDs480 (Inset: corresponding particle size distribution of the Ru nanoparticles). Adapted with permission [222]. Copyright 2018, Wiley. (**c1**) Schematic illustration of the synthesis of the Ru@PC, Ru@CQDs and Ru@P-AC, (**c2**) TEM, HRTEM image and schematic illustration of Ru@PC, Ru@CQDs and Ru@P-AC. Adapted with permission [223]. Copyright 2020, Royal Society of Chemistry.

NPs (Rh/Ni@NCNTs) was obtained [230]. The Rh and Ni NPs with size of ~ 1.92 nm and ~ 18.56 nm was highly dispersed on the surface of carbon nanotube which was expected to provide more active sites. The Rh/Ni@NCNTs showed excellent HER performance in a range of universal-pH, even exceed the commercial Pt/C. In addition of carbon matrix to support Rh NPs, using the phosphide of Rh is another potential protocol to synthesize an efficient electrocatalysts for HER. Liu' group [231] has demonstrated a novel supramolecular starch-assisted confinement-assembly-pyrolysis (SCAP) strategy to synthesize Rh_2P NPs anchored on N and P co-doped porous carbon (Rh_2P/NPC) (Fig. 16a1). The molecular structure contains abundant hydroxyl groups of starch was the stabilizer of metal ions aggregating in the synthesize process. The highly dispersed Ru_2P NPs ensure the robust activity of Ru_2P/NPC. Through FT-EXAFS measurement, the strong interaction between the Rh-P site and H_2O have been proved to be the positive role in HER process (Fig. 16a2). DFT results reveled the hydrogen bonding energy of Rh-P site was −0.06 eV, further confirming the high HER activity of Ru_2P/NPC (Fig. 16a3).

As a less expensive noble metal, silver (Ag) can be one of choice to prepare electrocatalysts to replace Pt [232]. Sun's group [233] have prepared P-doped Ag nanoparticles embedded in N-doped carbon (P-Ag@NC) via thermal-annealing and phosphorization using the glucose as the biomass precursor. The (111), (200), (220) and (311) crystal planes of metallic Ag were proved by XRD patterns. The slightly shifted of higher Bragg angle have revealed the existence of P dopants. The P-Ag@NC exhibited excellent HER behaviors with 78 mV to drive the current density to 10 mA cm^{-2}, 198 mV lower than Ag@NC (without P doping). The $\triangle G_{H^*}$ value decreased slightly due to the combination of metallic Ag with NC. The $\triangle G_{H^*}$ value was further decreased after successfully doping into the Ag@NC of P atoms, and thus resulted in an great electrocatalytic activity for HER. To introduce the heteroatoms combining with the metallic sites is an efficient method to improve the HER activity of hybrid catalysts.

The research of utilizing Aurum (Au) to catalytic HER in the electrochemical process was rarely reported, due to its relatively large hydrogen bonding energy. Through an environmental process of bio-reduction, Zhou et al. [234] prepared the Au decorated N-doped carbon (Au@NC). As presented in Fig. 17a1 and a2, the Au ions trapped by microorganism cell wall and cytoplasm was reduced into Au NPs via proteins/enzyme. The Au NPs loaded on the N-doped carbon substrate with a size range from 10 ~ 40 nm after the process of being annealed in Ar. The overpotential to drive the current density to 10 mA cm^{-2} was about 130 mV in 0.5 M H_2SO_4. There was no chemical reductant involved in the bioreduction process. The conversion process demonstrated an appealing protocol to acquire functional carbon materials from biomass.

The natural abundance, modifiable, and easily functionalized of the biomass-based carbon material and TM have drawn an extensive

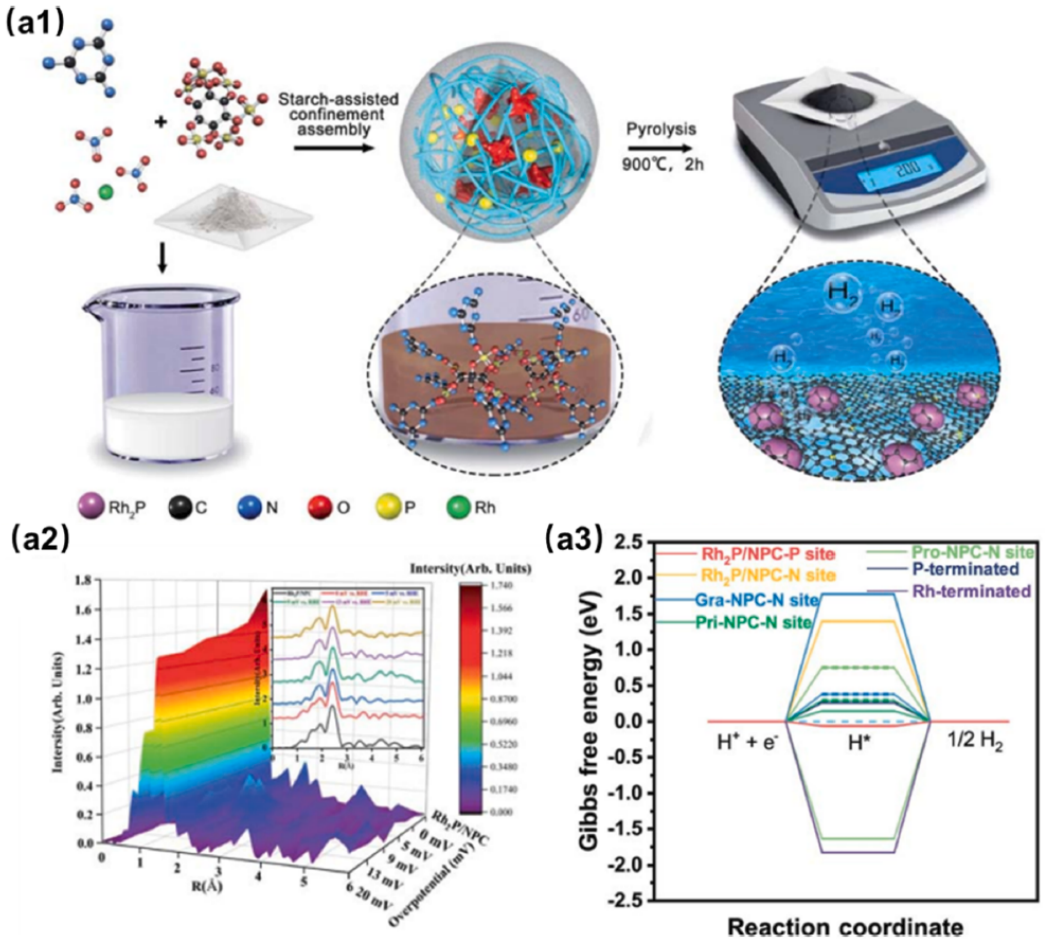

Fig. 16. (a1) Schematic illustration of the preparation process of the Rh_2P/NPC catalyst, (a2) FT-EXAFS spectra of the Rh_2P/NPC catalyst at different overpotentials, (a3) Gibbs free energy diagrams for the HER on NPC, Rh_2P and Rh_2P/NPC (Gra-NPC, Pri-NPC and Pro-NPC denote graphitic, pyridinic and pyrrolic NPC, respectively). Adapted with permission [231]. Copyright 2018, Royal Society of Chemistry.

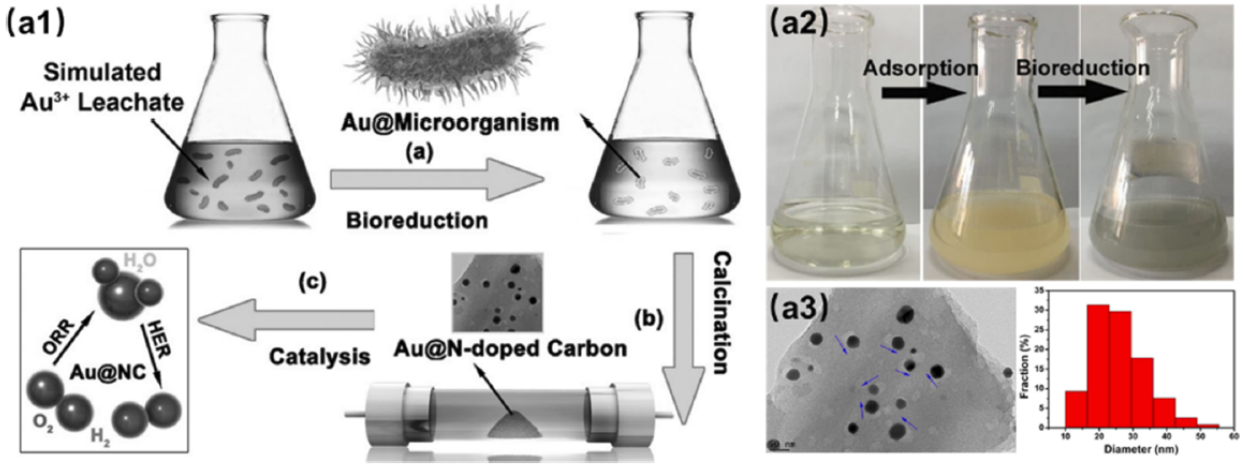

Fig. 17. (a1) Illustration of the conversion process of Au@NC, (a2) Adsorption and bioreduction of Au ions, (a3) TEM images of Au@NC (The arrows show the movement of the Au nanoparticles.) and the size distribution histogram of Au nanoparticles, Adapted with permission[234]. Copyright 2016, Wiley.

attention in electrochemistry fields. With rational design, the biomass-derived carbon hybrid with TM can be prepared as a HER electrocatalysts. Among the discussion above, the HER electrocatalysts consisted of biomass-derived carbon material which decorated with the TM showed enhancement performance in HER compared with pristine biomass-derived carbon material as shown in Table 1. Some of them showed an outstanding electrocatalytic activity for HER and even could be a promise substitutes to precious metal catalysts [58,128,146,147,150,179,180]. The overpotential at 10 mA cm^{-2} for such hybrid electrocatalysts is smaller than 100 mV. Among these hybrid catalysts, the spiky-like Mo_2C synthesized using the birch tree has the smallest value of η_{10} (35 mV) [150]. Especially, when the biomass-based carbon material was modified via trace amount of *Ru*, the overpotential to afford a current density to 10 mA cm^{-2} is only 24.6 mV and 10 mV respectively, which is exceed the electrocatalytic performance of commercial Pt/C [222]. In fact, The noble metals are still the most active electrocatalysts for HER due to its most suitable value of $\triangle G_{H^*}$, which results in an low overpotential and fast kinetics to drive HER. Since the scarcity and high cost limit the extensive utilization. As the cheapest metal among Pt-group metals, to design the electrocatalysts using trace Ru is a promised method.

5. Conclusions

The natural organic components and microstructure of biomass can promote the self-doping of heteroatoms or the in-situ transformation of morphological structure through a simple preparation strategy. For metal-free catalysts, the electrocatalytic activity of the metal-free electrocatalysts is related to specific surface area, porosity, surface defects, active centers and heteroatom doping. When the biomass-derived carbon material is loaded with metals and their compounds, abundant surface functional groups, pores, and heteroatoms will promote the anchoring of metals and their compounds. During the electrochemical process, the biomass-derived matrix protects the metal particles from corrosion and aggregation. The synergistic effect between heteroatoms and metals can significantly optimize $\triangle G_{H^*}$, improving the HER performance. It is remarkable that the hybrid catalyst decorated with the Ru NPs exhibits a prominent performance regardless of commercial Pt/C.

With regarding to the above discussion, the challenges of this area are carefully addressed as follows:1) The conversion mechanism (especially, the defects, active sites, etc.) of the biomass precursor into final carbon material, 2) The directional and controllable preparation of carbon-based electrocatalysts derived from biomass for hydrogen evolution, 3) Anchoring the metals on biomass-derived carbon matrix by in-situ growth, 4) The new structure and electrocatalytic performance of catalyst, 5) The synergetic effect between the heteroatom and metal and its enhancement, 6) Integration of electrocatalytic HER equipment with renewable energy configurations to test the HER performance of the catalyst (such as the generation speed hydrogen bubbles, duration, etc.) and evaluating the energy efficiency of the system.

Declaration of Competing Interest

The authors declare that they have no known competing financial interests or personal relationships that could have appeared to influence the work reported in this paper.

Acknowledgements

The authors gratefully acknowledge the support of National Natural Science Foundation (51878145 and 51861145102), and Jiangsu Provincial Key Research and Development Program (BE2020114).

References

[1] Nathan S, Lewis DGN. Powering the planet: Powering the planet: Chemical challenges in solar energy utilization. Proc Natl Acad Sci U S A 2007;103(43):15729–35.
[2] Renewables 2018 Global Status Report, 2018, pp. REN21; Renewables 2018 Global Status Report.
[3] Dai L, Chang DW, Baek JB, Lu W. Carbon nanomaterials for advanced energy conversion and storage. Small 2012;8(8):1130–66.
[4] Deng J, Li M, Wang Y. Biomass-derived carbon: synthesis and applications in energy storage and conversion. Green Chem 2016;18(18):4824–54.
[5] A national vision of America's Transition to a Hydrogen Economy To 2030 and Beyond, in: U.S.D.o. Energy (Ed.) Washington, DC, 2003.
[6] Zhu J, Hu L, Zhao P, Lee LYS, Wong KY. Recent advances in electrocatalytic hydrogen evolution using nanoparticles. Chem Rev 2020;120(2):851–918.
[7] Jaramillo TF, Jørgensen KP, Bonde J, Nielsen JH, Horch S, Chorkendorff I. Identification of active edge sites for electrochemical H_2 evolution from MoS_2 nanocatalysts. Science 2007;317(5834):100–2.
[8] Nørskov JK, Bligaard T, Logadottir A, Kitchin JR, Chen JG, Pandelov S. Stimming, Trends in the exchange current for hydrogen evolution. J Electrochem Soc 2005;152(3):J23–6.
[9] Li H, Tang Q, He B, Yang P. Robust electrocatalysts from an alloyed Pt-Ru-M (M = Cr, Fe Co, Ni, Mo)-decorated Ti mesh for hydrogen evolution by seawater splitting. J Mater Chem A 2016;4(17):6513–20.
[10] Guo W, Lv H, Chen Z, Sullivan KP, Lauinger SM, Chi Y, et al. Self-assembly of polyoxometalates, Pt nanoparticles and metal-organic frameworks into a hybrid material for synergistic hydrogen evolution. J Mater Chem A 2016;4(16):5952–7.
[11] Prabu N, Saravanan RSA, Kesavan T, Maduraiveeran G, Sasidharan M. An efficient palm waste derived hierarchical porous carbon for electrocatalytic hydrogen evolution reaction. Carbon 2019;152:188–97.

[12] Sun T, Zhang C, Chen J, Yan Y, Zakhidov AA, Baughman RH, et al. Three-dimensionally ordered macro-/mesoporous Ni as a highly efficient electrocatalyst for the hydrogen evolution reaction. J Mater Chem A 2015;3(21):11367–75.

[13] Xu L-H, Zhang S-L, Guo S-Y, Zhang X-J, Cosnier S, Marks RS, et al. ATMP derived cobalt-metaphosphate complex as highly active catalyst for oxygen reduction reaction. J Catal 2020;387:129–37.

[14] Xu L-H, Zeng H-B, Zhang X-J, Cosnier S, Marks RS, Shan D. Highly active $M_2P_2O_7$@NC (M = Co and Zn) for bifunctional electrocatalysts for ORR and HER. J Catal 2019;377:20–7.

[15] McKone JR, Sadtler BF, Werlang CA, Lewis NS, Gray HB. Ni-Mo nanopowders for efficient electrochemical hydrogen evolution. ACS Catal 2013;3(2):166–9.

[16] Yang L, Zhou W, Hou D, Zhou K, Li G, Tang Z, et al. Porous metallic MoO_2-supported MoS_2 nanosheets for enhanced electrocatalytic activity in the hydrogen evolution reaction. Nanoscale 2015;7(12):5203–8.

[17] Yang L, Yu J, Wei Z, Li G, Cao L, Zhou W, et al. Co-N-doped MoO_2 nanowires as efficient electrocatalysts for the oxygen reduction reaction and hydrogen evolution reaction. Nano Energy 2017;41:772–9.

[18] Ma L, Hu Y, Chen R, Zhu G, Chen T, Lv H, et al. Self-assembled ultrathin $NiCo_2S_4$ nanoflakes grown on Ni foam as high-performance flexible electrodes for hydrogen evolution reaction in alkaline solution. Nano Energy 2016;24:139–47.

[19] Reddy S, Du R, Kang L, Mao N, Zhang J. Three dimensional CNTs aerogel/MoSx as an electrocatalyst for hydrogen evolution reaction. Appl Catal B 2016;194:16–21.

[20] Peng S, Li L, Han X, Sun W, Srinivasan M, Mhaisalkar SG, et al. Cobalt sulfide nanosheet/graphene/carbon nanotube nanocomposites as flexible electrodes for hydrogen evolution. Angew Chem Int Ed 2014;53(46):12594–9.

[21] Wang T, Liu L, Zhu Z, Papakonstantinou P, Hu J, Liu H, et al. Enhanced electrocatalytic activity for hydrogen evolution reaction from self-assembled monodispersed molybdenum sulfidenanoparticles on an Au electrode. Energy Environ Sci 2013;6(2):625–33.

[22] Wang J, Gao D, Wang G, Miao S, Wu H, Li J, et al. Cobalt nanoparticles encapsulated in nitrogen-doped carbon as a bifunctional catalyst for water electrolysis. J Mater Chem A 2014;2(47):20067–74.

[23] Zhang H, Ma Z, Duan J, Liu H, Liu G, Wang T, et al. Active sites implanted carbon cages in core-shell architecture: highly active and durable electrocatalyst for hydrogen evolution reaction. ACS Nano 2016;10(1):684–94.

[24] Yi Shen YZ, Duo Wang, Xi Wu, Jia Li, and Jingyu Xi. Nickel-copper alloy encapsulated in graphitic carbon shells as electrocatalysts for hydrogen evolution reaction. Adv Energy Mater 2017;1701759:7.

[25] Chen L, Yang S, Qian K, Wei W, Sun C, Xie J. In situ growth of N-doped carbon coated CoNi alloy with graphene decoration for enhanced HER performance. J Energy Chem 2019;29:129–35.

[26] Park S-W, Kim I, Oh S-I, Kim J-C, Kim D-W. Carbon-encapsulated NiFe nanoparticles as a bifunctional electrocatalyst for high-efficiency overall water splitting. J Catal 2018;366:266–74.

[27] Deng J, Ren P, Deng D, Yu L, Yang F, Bao X. Highly active and durable non-precious-metal catalysts encapsulated in carbon nanotubes for hydrogen evolution reaction. Energy Environ Sci 2014;7(6):1919–23.

[28] Du B, Meng Q-T, Sha J-Q, Li J-S. Facile synthesis of FeCo alloys encapsulated in nitrogen-doped graphite/carbon nanotube hybrids: efficient bi-functional electrocatalysts for oxygen and hydrogen evolution reactions. New J Chem 2018;42(5):3409–14.

[29] Feng X, Bo X, Guo L. CoM (M = Fe, Cu, Ni)-embedded nitrogen-enriched porous carbon framework for efficient oxygen and hydrogen evolution reactions. J Power Sources 2018;389:249–59.

[30] Horvat I, Dović D. Combustion of Agricultural Biomass-Issues and Solutions. Transactions of FAMENA 2018;42(Si1):75–86.

[31] Supanchaiyamat N, Jetsrisuparb K, Knijnenburg JTN, Tsang DCW, Hunt AJ. Lignin materials for adsorption: Current trend, perspectives and opportunities. Bioresour Technol 2019;272:570–81.

[32] Shen J, Wu H, Sun W, Wu Q, Zhen S, Wang Z, et al. Biomass-derived hierarchically porous carbon skeletons with in situ decorated IrCo nanoparticles as high-performance cathode catalysts for Li-O2 batteries. J Mater Chem A 2019;7(17):10662–71.

[33] Lai X, Halpert JE, Wang D. Recent advances in micro-/nano-structured hollow spheres for energy applications: From simple to complex systems. Energy Environ Sci 2012;5(2):5604–18.

[34] Gao S, Li X, Li L, Wei X. A versatile biomass derived carbon material for oxygen reduction reaction, supercapacitors and oil/water separation. Nano Energy 2017;33:334–42.

[35] Zhang Z, Yang S, Li H, Zan Y, Li X, Zhu Y, et al. Sustainable carbonaceous materials derived from biomass as metal-free electrocatalysts. Adv Mater 2019;31(13):e1805718.

[36] Yang L, Zeng X, Wang D, Cao D. Biomass-derived FeNi alloy and nitrogen-codoped porous carbons as highly efficient oxygen reduction and evolution bifunctional electrocatalysts for rechargeable Zn-air battery. Energy Storage Mater 2018;12:277–83.

[37] White RJ, Budarin V, Luque R, Clark JH, Macquarrie DJ. Tuneable porous carbonaceous materials from renewable resources. Chem Soc Rev 2009;38(12):3401–18.

[38] Gong Y, Li D, Luo C, Fu Q, Pan C. Highly porous graphitic biomass carbon as advanced electrode materials for supercapacitors. Green Chem 2017;19(17):4132–40.

[39] Dutta S, Bhaumik A, Wu KCW. Hierarchically porous carbon derived from polymers and biomass: effect of interconnected pores on energy applications. Energy Environ Sci 2014;7(11):3574–92.

[40] Ren J, Zhou Y, Wu H, Xie F, Xu C, Lin D. Sulfur-encapsulated in heteroatom-doped hierarchical porous carbon derived from goat hair for high performance lithium-sulfur batteries. J Energy Chem 2019;30:121–31.

[41] Qian W, Sun F, Xu Y, Qiu L, Liu C, Wang S, et al. Human hair-derived carbon flakes for electrochemical supercapacitors. Energy Environ Sci 2014;7(1):379–86.

[42] Liu Z, Li Z, Tian S, Wang M, Sun H, Liang S, et al. Conversion of peanut biomass into electrocatalysts with vitamin B12 for oxygen reduction reaction in Zn-air battery. Int J Hydrogen Energy 2019;44(23):11788–96.

[43] Wang M, Ma J, Yang H, Lu G, Yang S, Chang Z. Nitrogen and cobalt co-doped carbon materials derived from biomass chitin as high-performance electrocatalyst for aluminum-air batteries. Catalysts 2019;9(11):954.

[44] Mao X, Cao Z, Chen S, Jia J, Li X, Yin Y, et al. Facile synthesis of N, P-doped hierarchical porous carbon framework catalysts based on gelatin/phytic acid supermolecules for electrocatalytic oxygen reduction. Int J Hydrogen Energy 2019;44(12):5890–8.

[45] Zhang G, Wang G, Liu Y, Liu H, Qu J, Li J. Highly active and stable catalysts of phytic acid-derivative transition metal phosphides for full water splitting. J Am Chem Soc 2016;138(44):14686–93.

[46] Ito Y, Cong W, Fujita T, Tang Z, Chen M. High catalytic activity of nitrogen and sulfur co-doped nanoporous graphene in the hydrogen evolution reaction. Angew Chem Int Ed 2015;54(7):2131–6.

[47] Jiao Y, Zheng Y, Davey K, Qiao S-Z. Activity origin and catalyst design principles for electrocatalytic hydrogen evolution on heteroatom-doped graphene. Nat Energy 2016;1(10):1–9.

[48] Zhang J, Chen G, Mullen K, Feng X. Carbon-rich nanomaterials: fascinating hydrogen and oxygen electrocatalysts. Adv Mater 2018;30(40):e1800528.

[49] Wang G, Zhang L, Zhang J. A review of electrode materials for electrochemical supercapacitors. Chem Soc Rev 2012;41(2):797–828.

[50] Li G, Yu J, Jia J, Yang L, Zhao L, Zhou W, et al. Cobalt-Cobalt Phosphide Nanoparticles@Nitrogen-Phosphorus Doped Carbon/Graphene Derived from Cobalt Ions Adsorbed Saccharomycete Yeasts as an Efficient, Stable, and Large-Current-Density Electrode for Hydrogen Evolution Reactions. Adv Funct Mater 2018;28(40):1801332.

[51] Li G, Wang J, Yu J, Liu H, Cao Q, Du J, et al. Ni-Ni_3P nanoparticles embedded into N, P-doped carbon on 3D graphene frameworks via in situ phosphatization of saccharomycetes with multifunctional electrodes for electrocatalytic hydrogen production and anodic degradation. Appl Catal B 2020;261:118147.

[52] Yu J, Li G, Liu H, Zhao L, Wang A, Liu Z, et al. Ru–Ru2PΦNPC and NPC@RuO2 Synthesized via Environment-Friendly and Solid-Phase Phosphating Process by Saccharomycetes as N/P Sources and Carbon Template for Overall Water Splitting in Acid Electrolyte. Adv Funct Mater 2019;29(22):1901154.

[53] Meng W, Bai X, Wang B, Liu Z, Lu S, Yang B. Biomass-Derived Carbon Dots and Their Applications. Energy Environ Mater 2019;2(3):172–92.

[54] Wu Z-Y, Hu B-C, Wu P, Liang H-W, Yu Z-L, Lin Y, et al. Mo_2C nanoparticles embedded within bacterial cellulose-derived 3D N-doped carbon nanofiber networks for efficient hydrogen evolution. NPG Asia Mater 2016;8(7):e288.

[55] Mu Y, Zhang Y, Fang L, Liu L, Zhang H, Wang Y. Controllable synthesis of molybdenum carbide nanoparticles embedded in porous graphitized carbon matrixes as efficient electrocatalyst for hydrogen evolution reaction. Electrochim Acta 2016;215:357–65.

[56] Meng F, Hu E, Zhang L, Sasaki K, Muckerman JT, Fujita E. Biomass-derived high-performance tungsten-based electrocatalysts on graphene for hydrogen evolution. J Mater Chem A 2015;3(36):18572–7.

[57] Jin H, Wang J, Su D, Wei Z, Pang Z, Wang Y. In situ cobalt-cobalt oxide/N-doped carbon hybrids as superior bifunctional electrocatalysts for hydrogen and oxygen evolution. J Am Chem Soc 2015;137(7):2688–94.

[58] Zhang TQ, Liu J, Huang LB, Zhang XD, Sun YG, Liu XC, et al. Microbial-phosphorus-enabled synthesis of phosphide nanocomposites for efficient electrocatalysts. J Am Chem Soc 2017;139(32):11248–53.

[59] Jiang F, Yao Y, Natarajan B, Yang C, Gao T, Xie H, et al. Ultrahigh-temperature conversion of biomass to highly conductive graphitic carbon. Carbon 2019;144:241–8.

[60] Maldonado-Hódar FJ, Moreno-Castilla C, Rivera-Utrilla J, Hanzawa Y, Yamada Y. Catalytic graphitization of carbon aerogels by transition metals. Langmuir 2000;16(9):4367-73.

[61] Thompson E, Danks AE, Bourgeois L, Schnepp Z. Iron-catalyzed graphitization of biomass. Green Chem 2015;17(1):551–6.

[62] Borghei M, Laocharoen N, Kibena-Põldsepp E, Johansson L-S, Campbell J, Kauppinen E, et al. Porous N, P-doped carbon from coconut shells with high electrocatalytic activity for oxygen reduction: Alternative to Pt-C for alkaline fuel cells. Appl Catal B 2017;204:394–402.

[63] Tang Z, Pei Z, Wang Z, Li H, Zeng J, Ruan Z, et al. Highly anisotropic, multichannel wood carbon with optimized heteroatom doping for supercapacitor and oxygen reduction reaction. Carbon 2018;130:532–43.

[64] Gong K, Du F, Xia ZH, Durstock M, Dai L. Nitrogen-doped carbon nanotube arrays with high electrocatalytic activity for oxygen reduction. Science 2009;323(5915):760–4.

[65] Ashokkumar M, Narayanan NT, Mohana Reddy AL, Gupta BK, Chandrasekaran B, Talapatra S, et al. Transforming collagen wastes into doped nanocarbons for sustainable energy applications. Green Chem 2012;14(6):1689–95.

[66] Zhu H, Yin J, Wang X, Wang H, Yang X. Microorganism-derived heteroatom-doped carbon materials for oxygen reduction and supercapacitors. Adv Funct Mater 2013;23(10):1305–12.

[67] Gao S, Fan H, Zhang S. Nitrogen-enriched carbon from bamboo fungus with superior oxygen reduction reaction activity. J Mater Chem A 2014;2(43):18263–70.

[68] Brun N, Wohlgemuth SA, Osiceanu P, Titirici MM. Original design of nitrogen-doped carbon aerogels from sustainable precursors: application as metal-free oxygen reduction catalysts. Green Chem 2013;15(9):2514–24.

[69] Liang H-W, Wu Z-Y, Chen L-F, Li C, Yu S-H. Bacterial cellulose derived nitrogen-doped carbon nanofiber aerogel: An efficient metal-free oxygen reduction electrocatalyst for zinc-air battery. Nano Energy 2015;11:366–76.

[70] Park SY, Lee HU, Park ES, Lee SC, Lee JW, Jeong SW, et al. Photoluminescent green carbon nanodots from food-waste-derived sources: large-scale synthesis, properties, and biomedical applications. ACS Appl Mater Interfaces 2014;6(5):3365–70.

[71] Li L, Diederick R, Flora JR, Berge ND. Hydrothermal carbonization of food waste and associated packaging materials for energy source generation. Waste Manage 2013;33(11):2478–92.

[72] Ding J, Wang H, Li Z, Cui K, Karpuzov D, Tan X, et al. Peanut shell hybrid sodium ion capacitor with extreme energy-power rivals lithium ion capacitors. Energy Environ Sci 2015;8(3):941–55.

[73] Saravanan KRA, Prabu N, Sasidharan M, Maduraiveeran G. Nitrogen-self doped activated carbon nanosheets derived from peanut shells for enhanced hydrogen evolution reaction. Appl Surf Sci 2019;489:725–33.

[74] Lv W, Wen F, Xiang J, Zhao J, Li L, Wang L, et al. Peanut shell derived hard carbon as ultralong cycling anodes for lithium and sodium batteries. Electrochim Acta 2015;176:533–41.

[75] Liu Y, Yu H, Quan X, Chen S, Zhao H, Zhang Y. Efficient and durable hydrogen evolution electrocatalyst based on nonmetallic nitrogen doped hexagonal carbon. Sci Rep 2014;4:6843.

[76] Chen Y, Li J, Mei T, Xg Hu, Liu D, Wang J, et al. Low-temperature and one-pot synthesis of sulfurized graphene nanosheets via in situ doping and their superior electrocatalytic activity for oxygen reduction reaction. J Mater Chem A 2014;2(48):20714–22.

[77] Liang HW, Bruller S, Dong R, Zhang J, Feng X, Mullen K. Molecular metal-Nx centres in porous carbon for electrocatalytic hydrogen evolution. Nat Commun 2015;6:7992.

[78] Zheng Y, Jiao Y, Li LH, Xing T, Chen Y, Jaroniec M, et al. Toward Design of Synergistically Active Carbon-Based Catalysts for Electrocatalytic Hydrogen Evolution. ACS Nano 2014;8(5):5290–6.

[79] Yang J, Voiry D, Ahn SJ, Kang D, Kim AY, Chhowalla M, et al. Two-dimensional hybrid nanosheets of tungsten disulfide and reduced graphene oxide as catalysts for enhanced hydrogen evolution. Angew Chem Int Ed 2013;52(51):13751–4.

[80] Peng Y, Lu B, Chen L, Wang N, Lu JE, Ping Y, et al. Hydrogen evolution reaction catalyzed by ruthenium ion-complexed graphitic carbon nitride nanosheets. J Mater Chem A 2017;5(34):18261–9.

[81] Pels JR, Kapteijn F, Moulijn JA, Zhu Q, Thomas KM. Evolution of nitrogen functionalities in carbonaceous materials during pyrolysis. Carbon 1995;33(11):1641–53.

[82] Schmiers H, Friebela F, Streubel P, Hesse R, Köpsela R. Change of chemical bonding of nitrogen of polymeric Nheterocyclic compounds during pyrolysis. Carbon 1999;37(12):1965–78.

[83] Zhu G, Ma L, Lv H, Hu Y, Chen T, Chen R, et al. Pine needle-derived microporous nitrogen-doped carbon frameworks exhibit high performances in electrocatalytic hydrogen evolution reaction and supercapacitors. Nanoscale 2017;9(3):1237–43.

[84] Liu X, Zhang M, Yu D, Li T, Wan M, Zhu H, et al. Functional materials from nature: honeycomb-like carbon nanosheets derived from silk cocoon as excellent electrocatalysts for hydrogen evolution reaction. Electrochim. Acta 2016;215:223–30.

[85] Li F, Yang J, Liao J, Li S, Liao J, Prabhu R, et al. Direct synthesis of carbon-based microtubes by hydrothermal carbonization of microorganism cells. Chem Eng J 2015;276:322–30.

[86] Huang B, Liu Y, Xie Z. Biomass derived 2D carbonsviaa hydrothermal carbonization method as efficient bifunctional ORR/HER electrocatalysts. J Mater Chem A 2017;5(45):23481–8.

[87] Nsabimana A, Wu F, Lai J, Liu Z, Luque R, Xu G. Simple synthesis of nitrogen-doped porous carbon from Chinese steamed bread flour and its catalytic application for hydrogen evolution reaction. Electrochim Acta 2018;290:30–7.

[88] Prabu N, Kesavan T, Maduraiveeran G, Sasidharan M. Bio-derived nanoporous activated carbon sheets as electrocatalyst for enhanced electrochemical water splitting. Int J Hydrogen Energy 2019;44(36):19995–20006.

[89] Jiang H, Gu J, Zheng X, Liu M, Qiu X, Wang L, et al. Defect-rich and ultrathin N doped carbon nanosheets as advanced trifunctional metal-free electrocatalysts for the ORR. OER and HER. Energy Environ Sci 2019;12(1):322–33.

[90] Zhou Y, Leng Y, Zhou W, Huang J, Zhao M, Zhan J, et al. Sulfur and nitrogen self-doped carbon nanosheets derived from peanut root nodules as high-efficiency non-metal electrocatalyst for hydrogen evolution reaction. Nano Energy 2015;16:357–66.

[91] Xie J, Zhang H, Li S, Wang R, Sun X, Zhou M, et al. Defect-rich MoS_2 ultrathin nanosheets with additional active edge sites for enhanced electrocatalytic hydrogen evolution. Adv Mater 2013;25(40):5807–13.

[92] Voiry D, Yamaguchi H, Li J, Silva R, Alves DC, Fujita T, et al. Enhanced catalytic activity in strained chemically exfoliated WS_2 nanosheets for hydrogen evolution. Nat Mater 2013;12(9):850–5.

[93] Zhao Y, Zhao F, Wang X, Xu C, Zhang Z, Shi G, et al. Graphitic carbon nitride nanoribbons: graphene-assisted formation and synergic function for highly efficient hydrogen evolution. Angew Chem Int Ed 2014;53(50):13934–9.

[94] Liu X, Zhou W, Yang L, Li L, Zhang Z, Ke Y, et al. Nitrogen and sulfur co-doped porous carbon derived from human hair as highly efficient metal-free electrocatalysts for hydrogen evolution reactions. J Mater Chem A 2015;3(16):8840–6.

[95] Liu Y, Hu M, Xu W, Wu X, Jiang J. Catalytically active carbon from cattail fibers for electrochemical reduction reaction. Front Chem 2019;7:786.

[96] Mulyadi A, Zhang Z, Dutzer M, Liu W, Deng Y. Facile approach for synthesis of doped carbon electrocatalyst from cellulose nanofibrils toward high-performance metal-free oxygen reduction and hydrogen evolution. Nano Energy 2017;32:336–46.

[97] Zhou G, Yang Q, Guo X, Chen Y, Yang Q, Xu L, et al. Coupling molybdenum carbide nanoparticles with N-doped carbon nanosheets as a high-efficiency electrocatalyst for hydrogen evolution reaction. Int J Hydrogen Energy 2018;43(19):9326–33.

[98] Xu YT, Xiao X, Ye ZM, Zhao S, Shen R, He CT, et al. Cage-Confinement Pyrolysis Route to Ultrasmall Tungsten Carbide Nanoparticles for Efficient Electrocatalytic Hydrogen Evolution. J Am Chem Soc 2017;139(15):5285–8.

[99] Fan H, Yu H, Zhang Y, Zheng Y, Luo Y, Dai Z, et al. Fe-Doped Ni_3C Nanodots in N-Doped Carbon Nanosheets for Efficient Hydrogen-Evolution and Oxygen-Evolution Electrocatalysis. Angew Chem Int Ed 2017;56(41):12566–70.

[100] Ouyang T, Ye YQ, Wu CY, Xiao K, Liu ZQ. Heterostructures Composed of N-Doped Carbon Nanotubes Encapsulating Cobalt and beta-Mo_2C Nanoparticles as Bifunctional Electrodes for Water Splitting. Angew Chem Int Ed 2019;58(15):4923–8.

[101] Xiong W, Guo Q, Guo Z, Li H, Zhao R, Chen Q, et al. Atomic layer deposition of nickel carbide for supercapacitors and electrocatalytic hydrogen evolution. J Mater Chem A 2018;6(10):4297–304.

[102] Levy RB, Boudart M. Platinum-like behavior of tungsten carbide in surface catalysis. Science 1973;181(4009):547–9.

[103] Bennett LH, Cuthill JR, Mcalister AJ, Erickson NE, Watson RE. Electronic structure and catalytic behavior of tungsten carbide. Science 1974;184(4136):563–5.

[104] Zhong X, Sun Y, Chen X, Zhuang G, Li X, Wang J-G. Mo Doping Induced More Active Sites in Urchin-Like $W_{18}O_{49}$ Nanostructure with Remarkably Enhanced Performance for Hydrogen Evolution Reaction. Adv Funct Mater 2016;26(32):5778–86.

[105] Song J, Huang Z-F, Pan L, Zou J-J, Zhang X, Wang L. Oxygen-Deficient Tungsten Oxide as Versatile and Efficient Hydrogenation Catalyst. ACS Catal 2015;5(11):6594–9.

[106] Kou Z, Wang T, Wu H, Zheng L, Mu S, Pan Z, et al. Twinned Tungsten Carbonitride Nanocrystals Boost Hydrogen Evolution Activity and Stability. Small 2019;15(19):e1900248.

[107] Fei H, Yang Y, Fan X, Wang G, Ruan G, Tour JM. Tungsten-based porous thin-films for electrocatalytic hydrogen generation. J Mater Chem. A 2015;3(11):5798–804.

[108] Ganesan R, Lee JS. Tungsten carbide microspheres as a noble-metal-economic electrocatalyst for methanol oxidation. Angew Chem Int Ed 2005;44(40):6557–60.

[109] Ji N, Zhang T, Zheng M, Wang A, Wang H, Wang X, et al. Direct catalytic conversion of cellulose into ethylene glycol using nickel-promoted tungsten carbide catalysts. Angew Chem Int Ed 2008;47(44):8510–3.

[110] Chen J, Yang H, Sang X, Su Z, Li D, Wang Q. Oxygen vacancy rich tungsten oxide with nitrogen doped mesoporous carbon as matrix for overall water splitting and 4-nitrophenol reductive removal. Solid State Sci 2018;83:23–30.

[111] Wang C, Tang J, Zhang X, Qian L, Yang H. WO_3 nanoflakes decorated with CuO clusters for enhanced photoelectrochemical water splitting. Prog Nat Sci: Mater Int 2018;28(2):200–4.

[112] Wondimu TH, Chen G-C, Kabtamu DM, Chen H-Y, Bayeh AW, Huang H-C, et al. Highly efficient and durable phosphine reduced iron-doped tungsten oxide/reduced graphene oxide nanocomposites for the hydrogen evolution reaction. Int J Hydrogen Energy 2018;43(13):6481–90.

[113] Chen J, Yu D, Liao W, Zheng M, Xiao L, Zhu H, et al. WO_3-x nanoplates grown on carbon nanofibers for an efficient electrocatalytic hydrogen evolution reaction. ACS Appl Mater Interfaces 2016;8(28):18132–9.

[114] Sekar S, Aqueel Ahmed AT, Pawar SM, Lee Y, Im H, Kim DY, et al. Enhanced water splitting performance of biomass activated carbon-anchored WO_3 nanoflakes. Appl Surf Sci 2020;508:145127.

[115] Wang B, Xu L, Liu G, Zhang P, Zhu W, Xia J, et al. Biomass willow catkin-derived Co_3O_4/N-doped hollow hierarchical porous carbon microtubes as an effective trifunctional electrocatalyst. J Mater Chem A 2017;5(38):20170–9.

[116] Faber MS, Dziedzic R, Lukowski MA, Kaiser NS, Ding Q, Jin S. High-performance electrocatalysis using metallic cobalt pyrite (CoS_2) micro-and nanostructures. J Am Chem Soc 2014;136(28):10053–61.

[117] Tian J, Liu Q, Asiri AM, Sun X. Self-supported nanoporous cobalt phosphide nanowire arrays: an efficient 3D hydrogen-evolving cathode over the wide range of pH 0–14. J Am Chem Soc 2014;136(21):7587–90.

[118] Hou D, Zhou W, Zhou K, Zhou Y, Zhong J, Yang L, et al. Flexible and porous catalyst electrodes constructed by Co nanoparticles@nitrogen-doped graphene films for highly efficient hydrogen evolution. J Mater Chem A 2015;3(31):15962–8.

[119] Liu S, Li L, Ahn HS, Manthiram A. Delineating the roles of Co_3O_4 and N-doped carbon nanoweb (CNW) in bifunctional Co_3O_4/CNW catalysts for oxygen reduction and oxygen evolution reactions. J Mater Chem A 2015;3(21):11615–23.

[120] Li Y, Wang G, Wei T, Fan Z, Yan P. Nitrogen and sulfur co-doped porous carbon nanosheets derived from willow catkin for supercapacitors. Nano Energy 2016;19:165–75.

[121] Zhang X, Liu R, Zang Y, Liu G, Wang G, Zhang Y, et al. Co/CoO nanoparticles immobilized on Co-N-doped carbon as trifunctional electrocatalysts for oxygen reduction, oxygen evolution and hydrogen evolution reactions. Chem Commun 2016;52(35):5946–9.

[122] Yang M, Wu D, Cheng D. Biomass-derived porous carbon supported Co/CoO yolk-shell nanoparticles as enhanced multifunctional electrocatalysts. Int J Hydrogen Energy 2019;44(13):6525–34.
[123] Liu R, Zhang H, Zhang X, Wu T, Zhao H, Wang G. Co_9S_8@N, P-doped porous carbon electrocatalyst using biomass-derived carbon nanodots as a precursor for overall water splitting in alkaline media. RSC Adv 2017;7(31):19181–8.
[124] Feng L-L, Fan M, Wu Y, Liu Y, Li G-D, Chen H, et al. Metallic Co_9S_8 nanosheets grown on carbon cloth as efficient binder-free electrocatalysts for the hydrogen evolution reaction in neutral media. J Mater Chem A 2016;4(18):6860–7.
[125] Feng LL, Li GD, Liu Y, Wu Y, Chen H, Wang Y, et al. Carbon-armored Co9S8 nanoparticles as all-pH efficient and durable H2-evolving electrocatalysts. ACS Appl Mater Interfaces 2015;7(1):980–8.
[126] Lin Y, Pan Y, Zhang J. CoP nanorods decorated biomass derived N, P co-doped carbon flakes as an efficient hybrid catalyst for electrochemical hydrogen evolution. Electrochim Acta 2017;232:561–9.
[127] Zhao W, Lu X, Selvaraj M, Wei W, Jiang Z, Ullah N, et al. MXP(M = Co/Ni) @carbon core-shell nanoparticles embedded in 3D cross-linked graphene aerogel derived from seaweed biomass for hydrogen evolution reaction. Nanoscale 2018;10(20):9698–706.
[128] Yuan W, Wang X, Zhong X, Li CM. CoP nanoparticles in situ grown in three-dimensional hierarchical nanoporous carbons as superior electrocatalysts for hydrogen evolution. ACS Appl Mater Interfaces 2016;8(32):20720–9.
[129] Yang M, Feng F, Wang K, Li S, Huang X, Gong L, et al. Synthesis of metal phosphide nanoparticles supported on porous N-doped carbon derived from spirulina for universal-pH hydrogen evolution. ChemSusChem 2020;13(2):351–9.
[130] Vrubel H, Hu X. Molybdenum boride and carbide catalyze hydrogen evolution in both acidic and basic solutions. Angew Chem Int Ed 2012;51(51):12703–6.
[131] Weidman MC, Esposito DV, Hsu Y-C, Chen JG. Comparison of electrochemical stability of transition metal carbides (WC, W_2C, Mo_2C) over a wide pH range. J Power Sources 2012;202:11–7.
[132] Ding Q, Song B, Xu P, Jin S. Efficient electrocatalytic and photoelectrochemical hydrogen generation using MoS_2 and related compounds. Chem 2016;1(5):699–726.
[133] Jia J, Zhou W, Wei Z, Xiong T, Li G, Zhao L, et al. Molybdenum carbide on hierarchical porous carbon synthesized from Cu-MoO_2 as efficient electrocatalysts for electrochemical hydrogen generation. Nano Energy 2017;41:749–57.
[134] Jin Y, Wang H, Li J, Yue X, Han Y, Shen PK, et al. Porous MoO_2 nanosheets as non-noble bifunctional electrocatalysts for overall water splitting. Adv Mater 2016;28(19):3785–90.
[135] Xiao P, Ge X, Wang H, Liu Z, Fisher A, Wang X. Novel Molybdenum carbide-tungsten carbide composite nanowires and their electrochemical activation for efficient and stable hydrogen evolution. Adv Funct Mater 2015;25(10):1520–6.
[136] Zhao Y, Kamiya K, Hashimoto K, Nakanishi S. Hydrogen evolution by tungsten carbonitride nanoelectrocatalysts synthesized by the formation of a tungsten acid/polymer hybrid in situ. Angew Chem Int Ed 2013;52(51):13638–41.
[137] Pu Z, Wang M, Kou Z, Amiinu IS, Mu S. Mo_2C quantum dot embedded chitosan-derived nitrogen-doped carbon for efficient hydrogen evolution in a broad pH range. Chem Commun 2016;52(86):12753–6.
[138] Kong X, Chen S, Zou Y, Lyu S, She X, Lu Y, et al. Cellulose nanocrystals (CNC) derived Mo_2C@sulfur-doped carbon aerogels for hydrogen evolution. Int J Hydrogen Energy 2018;43(30):13720–6.
[139] Nada AAMA, Hassan ML. Phosphorylated cation-exchangers from cotton stalks and their constituents. J Appl Polym Sci 2003;89(11):2950–6.
[140] Yang Y, Wang S, Zhang J, Li H, Tang Z, Wang X. Nanosheet-assembled $MoSe_2$ and S-doped MoSe2-x nanostructures for superior lithium storage properties and hydrogen evolution reactions. Inorg Chem Front 2015;2(10):931–7.
[141] Zeng JR, Gao MY, Zhang QB, Yang C, Li XT, Yang WQ, et al. Facile electrodeposition of cauliflower-like S-doped nickel microsphere films as highly active catalysts for electrochemical hydrogen evolution. J Mater Chem A 2017;5(29):15056–64.
[142] Ang H, Tan HT, Luo ZM, Zhang Y, Guo YY, Guo G, et al. Hydrophilic nitrogen and sulfur co-doped molybdenum carbide nanosheets for electrochemical hydrogen evolution. Small 2015;11(47):6278–84.
[143] Liang H-W, Guan Q-F, Zhu Z, Song L-T, Yao H-B, Lei X, et al. Highly conductive and stretchable conductors fabricated from bacterial cellulose. NPG Asia Mater 2012;4(6):e19-e.
[144] Chen L-F, Huang Z-H, Liang H-W, Gao H-L, Yu S-H. Three-dimensional heteroatom-doped carbon nanofiber networks derived from bacterial cellulose for supercapacitors. Adv Funct Mater 2014;24(32):5104–11.
[145] Wu Z-Y, Liang H-W, Li C, Hu B-C, Xu X-X, Wang Q, et al. Dyeing bacterial cellulose pellicles for energetic heteroatom doped carbon nanofiber aerogels. Nano Res 2014;7(12):1861–72.
[146] Wang J, Wei H, Chen X, Chen C, Xa Chen. Facile preparation of N, P co-doped molybdenum carbide/porous carbon rough microspheres for efficient electrocatalytic hydrogen evolution. Int J Hydrogen Energy 2020;45(1):595–604.
[147] An K, Xu X, Liu X. Mo_2C-based electrocatalyst with biomass-derived sulfur and nitrogen co-doped carbon as a matrix for hydrogen evolution and organic pollutant removal. ACS Sustainable Chem Eng 2017;6(1):1446–55.
[148] Yan Q, Yang X, Wei T, Zhou C, Wu W, Zeng L, et al. Porous beta-Mo_2C nanoparticle clusters supported on walnut shell powders derived carbon matrix for hydrogen evolution reaction. J Colloid Interface Sci 2020;563:104–11.
[149] Kou X, Chen Q, Li X, Li M, Kan C, Chen B, et al. Quantitative assessment of bioactive compounds and the antioxidant activity of 15 jujube cultivars. Food Chem 2015;173:1037–44.
[150] Humagain G, MacDougal K, MacInnis J, Lowe JM, Coridan RH, MacQuarrie S, et al. Highly efficient, biochar-derived molybdenum carbide hydrogen evolution electrocatalyst. Adv Energy Mater 2018;8(29)1801461.
[151] Zhang G, Liu H, Qu J, Li J. Two-dimensional layered MoS_2: rational design, properties and electrochemical applications. Energy Environ Sci 2016;9(4):1190–209.
[152] Benck JD, Hellstern TR, Kibsgaard J, Chakthranont P, Jaramillo TF. Catalyzing the hydrogen evolution reaction (HER) with molybdenum sulfide nanomaterials. ACS Catal 2014;4(11):3957–71.
[153] da Silveira Firmiano EG, Rabelo AC, Dalmaschio CJ, Pinheiro AN, Pereira EC, Schreiner WH, et al. Supercapacitor electrodes obtained by directly bonding 2D MoS_2 on reduced graphene oxide. Adv Energy Mater 2014;4(6):1301380.
[154] Bissett MA, Kinloch IA, Dryfe RA. Characterization of MoS_2-graphene composites for high-performance coin cell supercapacitors. ACS Appl Mater Interfaces 2015;7(31):17388–98.
[155] Sangeetha DN, Selvakumar M. Active-defective activated carbon/MoS_2 composites for supercapacitor and hydrogen evolution reactions. Appl Surf Sci 2018;453:132–40.
[156] Cai L, He J, Liu Q, Yao T, Chen L, Yan W, et al. Vacancy-induced ferromagnetism of MoS_2 nanosheets. J Am Chem Soc 2015;137(7):2622–7.
[157] Zhao X, Zhu H, Yang X. Amorphous carbon supported MoS_2 nanosheets as effective catalysts for electrocatalytic hydrogen evolution. Nanoscale 2014;6(18):10680–5.
[158] Qiao S, Zhao J, Zhang B, Liu C, Li Z, Hu S, et al. Micrometer-scale biomass carbon tube matrix auxiliary MoS_2 heterojunction for electrocatalytic hydrogen evolution. Int. J. Hydrogen Energy 2019;44(60):32019–29.
[159] Li K, Wang R, Chen J. Hydrodeoxygenation of anisole over silica-supported Ni2P, MoP, and NiMoP catalysts. Energy Fuels 2011;25(3):854–63.
[160] Whiffen VML, Smith KJ. A comparative study of 4-methylphenol hydrodeoxygenation over high surface area MoP and Ni_2P. Top Catal 2012;55(14–15):981–90.
[161] Ping Liu JAR. Catalytic properties of molybdenum carbide, nitride and phosphide: a theoretical study. Catal Lett 2003;91(3–4):247–52.
[162] Yao Z, Lai Z, Zhang X, Peng F, Yu H, Wang H. Structural stability and mutual transformations of molybdenum carbide, nitride and phosphide. Mater Res Bull 2011;46(11):1938–41.
[163] Song H, Li Y, Shang L, Tang Z, Zhang T, Lu S. Designed controllable nitrogen-doped carbon-dots-loaded MoP nanoparticles for boosting hydrogen evolution reaction in alkaline medium. Nano Energy 2020;72:104730.
[164] Cui W, Liu Q, Xing Z, Asiri AM, Alamry KA, Sun X. MoP nanosheets supported on biomass-derived carbon flake: One-step facile preparation and application as a novel high-active electrocatalyst toward hydrogen evolution reaction. Appl Catal B 2015;164:144–50.
[165] Kumar R, Rai R, Gautam S, De Sarkar A, Tiwari N, Jha SN, et al. Nano-structured hybrid molybdenum carbides/nitrides generated in situ for HER applications. J Mater Chem A 2017;5(17):7764–8.
[166] Chen J, Yang Y, Su J, Jiang P, Xia G, Chen Q. Enhanced Activity for Hydrogen Evolution Reaction over CoFe Catalysts by Alloying with Small Amount of Pt. ACS Appl Mater Interfaces 2017;9(4):3596–601.
[167] Chen YY, Zhang Y, Jiang WJ, Zhang X, Dai Z, Wan LJ, et al. Pomegranate-like N, P-Doped M_o2C@C nanospheres as highly active electrocatalysts for alkaline hydrogen evolution. ACS Nano 2016;10(9):8851–60.
[168] Chen W-F, Iyer S, Iyer S, Sasaki K, Wang C-H, Zhu Y, et al. Biomass-derived electrocatalytic composites for hydrogen evolution. Energy Environ Sci 2013;6(6):1818–26.
[169] Kumar R, Ahmed Z, Rai R, Gaur A, Kumari S, Maruyama T, et al. Uniformly decorated molybdenum carbide/nitride nanostructures on biomass templates for hydrogen evolution reaction applications. ACS Omega 2019;4(9):14155–61.
[170] Dresselhaus MS, Thomas IL. Alternative energy technologies. Nature 2001;414(6861):332–7.
[171] Hoang VC, Gomes VG, Dinh KN. Ni- and P-doped carbon from waste biomass: A sustainable multifunctional electrode for oxygen reduction oxygen evolution and hydrogen evolution reactions. Electrochim Acta 2019;314:49–60.
[172] Wang J, Mao S, Liu Z, Wei Z, Wang H, Chen Y, et al. Dominating role of Ni0 on the interface of Ni/NiO for enhanced hydrogen evolution reaction. ACS Appl Mater Interfaces 2017;9(8):7139–47.
[173] Hoang VC, Dinh KN, Gomes VG. Hybrid Ni/NiO composite with N-doped activated carbon from waste cauliflower leaves: A sustainable bifunctional electrocatalyst for efficient water splitting. Carbon 2020;157:515–24.
[174] Jiang L, Seong Y-H, Han SO, Kim H, Kim HH, Foord JS. Nickel treatment of biomass-derived nanocarbon for energy devices. Carbon 2018;130:724–9.
[175] Li T, Zhai Y, He SM, Gan WT, Wei ZY, Heidarinejad M, et al. A radiative cooling structural material. Science 2019;364:760–3.
[176] Chen C, Zhang Y, Li Y, Dai J, Song J, Yao Y, et al. All-wood, low tortuosity, aqueous, biodegradable supercapacitors with ultra-high capacitance. Energy Environ. Sci 2017;10(2):538–45.
[177] Peng X, Zhang L, Chen Z, Zhong L, Zhao D, Chi X, et al. Hierarchically Porous carbon plates derived from wood as bifunctional ORR/OER electrodes. Adv Mater 2019;31(16):e1900341.
[178] Hui B, Li G, Han G, Li Y, Wang L, Li J. Fabrication of magnetic response composite based on wood veneers by a simple in situ synthesis method. Wood Sci Technol 2015;49(4):755–67.
[179] Li Y, Gao T, Yao Y, Liu Z, Kuang Y, Chen C, et al. In situ "chainmail catalyst" assembly in low-tortuosity, hierarchical carbon frameworks for efficient and stable hydrogen generation. Adv Energy Mater 2018;8(25):1801289.

[180] Hui B, Zhang K, Xia Y, Zhou C. Natural multi-channeled wood frameworks for electrocatalytic hydrogen evolution. Electrochim Acta 2020;330:135274.
[181] Zhuang M, Ou X, Dou Y, Zhang L, Zhang Q, Wu R, et al. Polymer-embedded fabrication of Co_2P nanoparticles encapsulated in N, P-doped graphene for hydrogen generation. Nano Lett 2016;16(7):4691–8.
[182] Li L, Zhang G, Su Z. One-step assembly of phytic acid metal complexes for superhydrophilic coatings. Angew Chem Int Ed 2016;55(31):9093–6.
[183] Singh KP, Bae EJ, Yu JS. Fe-P: a new class of electroactive catalyst for oxygen reduction reaction. J Am Chem Soc 2015;137(9):3165–8.
[184] Pu Z, Amiinu IS, Zhang C, Wang M, Kou Z, Mu S. Phytic acid-derivative transition metal phosphides encapsulated in N, P-codoped carbon: an efficient and durable hydrogen evolution electrocatalyst in a wide pH range. Nanoscale 2017;9(10):3555–60.
[185] Li G, Yu J, Yu W, Yang L, Zhang X, Liu X, et al. Phosphorus-Doped Iron Nitride Nanoparticles Encapsulated by Nitrogen-Doped Carbon Nanosheets on Iron Foam In Situ Derived from Saccharomycetes Cerevisiae for Electrocatalytic Overall Water Splitting. Small 2020;16(32):e2001980.
[186] Feng J-J, Chen L-X, Ma X, Yuan J, Chen J-R, Wang A-J, et al. Bimetallic AuPt alloy nanodendrites/reduced graphene oxide: One-pot ionic liquid-assisted synthesis and excellent electrocatalysis towards hydrogen evolution and methanol oxidation reactions. Int J Hydrogen Energy 2017;42(2):1120–9.
[187] Redman DW, Rose MJ, Stevenson KJ. Electrodeposition of Amorphous Molybdenum chalcogenides from ionic liquids and their activity for the hydrogen evolution reaction. Langmuir 2017;33(37):9354–60.
[188] Xu J, Shi L, Liang C, Wu H, Lei J, Liu D, et al. Fe and N co-doped carbons derived from an ionic liquid as active bifunctional oxygen catalysts. ChemElectroChem 2017;4(5):1148–53.
[189] Li S, Dong Z, Yang H, Guo S, Gou G, Ren R, et al. Microenvironment effects in electrocatalysis: ionic-liquid-like coating on carbon nanotubes enhances the Pd-electrocatalytic alcohol oxidation. Chemistry 2013;19(7):2384–91.
[190] Li S, Guo S, Yang H, Gou G, Ren R, Li J, et al. Enhancing catalytic performance of Au catalysts by noncovalent functionalized graphene using functional ionic liquids. J Hazard Mater 2014;270:11–7.
[191] Gao J, Ma N, Zheng Y, Zhang J, Gui J, Guo C, et al. Cobalt/nitrogen-doped porous carbon nanosheets derived from polymerizable ionic liquids as bifunctional electrocatalyst for oxygen evolution and oxygen reduction reaction. ChemCatChem 2016;9(9):1601–9.
[192] Zhao X, Li S, Cheng H, Schmidt J, Thomas A. Ionic liquid-assisted synthesis of mesoporous carbons with surface-enriched nitrogen for the hydrogen evolution reaction. ACS Appl Mater Interfaces 2018;10(4):3912–20.
[193] Liu G, Wang B, Ding P, Ye Y, Wei W, Zhu W, et al. Reactable ionic liquid in situ-induced synthesis of Fe_3O_4 nanoparticles modified N-doped hollow porous carbon microtubes for boosting multifunctional electrocatalytic activity. J Alloys Compd 2019;797:849–58.
[194] Gupta S, Qiao L, Zhao S, Xu H, Lin Y, Devaguptapu SV, et al. Highly active and stable graphene tubes decorated with FeCoNi alloy nanoparticles via a template-free graphitization for bifunctional oxygen reduction and evolution. Adv Energy Mater 2016;6(22):1601198.
[195] Bayatsarmadi B, Zheng Y, Vasileff A, Qiao SZ. Recent advances in atomic metal doping of carbon-based nanomaterials for energy conversion. Small 2017;13(21):1700191.
[196] Fu G, Cui Z, Chen Y, Xu L, Tang Y, Goodenough JB. Hierarchically mesoporous nickel-iron nitride as a cost-efficient and highly durable electrocatalyst for Zn-air battery. Nano Energy 2017;39:77–85.
[197] Yang J, Wang X, Li B, Ma L, Shi L, Xiong Y, et al. Novel Iron/cobalt-containing polypyrrole hydrogel-derived trifunctional electrocatalyst for self-powered overall water splitting. Adv Funct Mater 2017;27(17):1606497.
[198] Deng WQ, Xu X, Goddard WA. A two-stage mechanism of bimetallic catalyzed growth of single-walled carbon nanotubes. Nano Lett 2004;4(12):2331–5.
[199] Wang J, Ciucci F. Boosting bifunctional oxygen electrolysis for N-doped carbon via bimetal addition. Small 2017;13(16):1604103.
[200] Wang J, Gao Y, You TL, Ciucci F. Bimetal-decorated nanocarbon as a superior electrocatalyst for overall water splitting. J Power Sources 2018;401:312–21.
[201] Kumar A, Chaudhary DK, Parvin S, Bhattacharyya S. High performance duckweed-derived carbon support to anchor NiFe electrocatalysts for efficient solar energy driven water splitting. J Mater Chem A 2018;6(39):18948–59.
[202] Kalyani P, Anitha A, Darchen A. Activated carbon from grass-A green alternative catalyst support for water electrolysis. Int J Hydrogen Energy 2013;38(25):10364–72.
[203] Palanichamy K, Ariharaputhiran A. Areca leaves as a source of carbon: Preliminary investigation as catalyst support for electrolytic hydrogen evolution in acidic medium. Int J Hydrogen Energy 2013;38(5):2263–70.
[204] Joshi U, Malkhandi S, Ren Y, Tan TL, Chiam SY, Yeo BS. Ruthenium-tungsten composite catalyst for the efficient and contamination-resistant electrochemical evolution of hydrogen. ACS Appl Mater Interfaces 2018;10(7):6354–60.
[205] Gao K, Wang Y, Wang Z, Zhu Z, Wang J, Luo Z, et al. Ru nanodendrites composed of ultrathin fcc/hcp nanoblades for the hydrogen evolution reaction in alkaline solutions. Chem Commun 2018;54(36):4613–6.
[206] Drouet S, Creus J, Colliere V, Amiens C, Garcia-Anton J, Sala X, et al. A porous Ru nanomaterial as an efficient electrocatalyst for the hydrogen evolution reaction under acidic and neutral conditions. Chem Commun 2017;53(85):11713–6.
[207] Zheng Y, Jiao Y, Zhu Y, Li LH, Han Y, Chen Y, et al. High electrocatalytic hydrogen evolution activity of an anomalous ruthenium catalyst. J Am Chem Soc 2016;138(49):16174–81.
[208] Udachyan I, Vishwanath RS, Pradeepa Kumara CS, Kandaiah S. Ruthenium ion containing N and S rich triazine based metallopolymer as a low overpotential acid stable electrocatalyst for hydrogen evolution. J Catal 2018;357:138–46.
[209] Barman BK, Das D, Nanda KK. Facile synthesis of ultrafine Ru nanocrystal supported N-doped graphene as an exceptional hydrogen evolution electrocatalyst in both alkaline and acidic media. Sustainable Energy Fuels 2017;1(5):1028–33.
[210] Li W, Zhao Y, Liu Y, Sun M, Waterhouse GIN, Huang B, et al. Exploiting Ru-induced Lattice Strain in CoRu Nanoalloys for Robust Bifunctional Hydrogen Production. Angew Chem Int Ed 2020.
[211] Zhang J, Liu P, Wang G, Zhang PP, Zhuang XD, Chen MW, et al. Ruthenium/nitrogen-doped carbon as an electrocatalyst for efficient hydrogen evolution in alkaline solution. J Mater Chem A 2017;5(48):25314–8.
[212] Zhang Z, Li P, Feng Q, Wei B, Deng C, Fan J, et al. Scalable synthesis of a ruthenium-based electrocatalyst as a promising alternative to Pt for hydrogen evolution reaction. ACS Appl Mater Interfaces 2018;10(38):32171–9.
[213] Liang T, Chen C, Li X, Zhang J. Popcorn-derived porous carbon for energy storage and CO_2 capture. Langmuir 2016;32(32):8042–9.
[214] Hou J, Jiang K, Wei R, Tahir M, Wu X, Shen M, et al. Popcorn-derived porous carbon flakes with an ultrahigh specific surface area for superior performance supercapacitors. ACS Appl Mater Interfaces 2017;9(36):30626–34.
[215] Luo D, Zhou B, Li Z, Qin X, Wen Y, Shi D, et al. Biomimetic organization of a ruthenium-doped collagen-based carbon scaffold for hydrogen evolution. J Mater Chem A 2018;6(5):2311–7.
[216] Wang B, Li J, Tang Z, Yang B, Lu S. Near-infrared emissive carbon dots with 33.96% emission in aqueous solution for cellular sensing and light-emitting diodes. Sci. Bull. 2019;64(17):1285–92.
[217] Song H, Liu X, Wang B, Tang Z, Lu S. High production-yield solid-state carbon dots with tunable photoluminescence for white/multi-color light-emitting diodes. Sci. Bull. 2019;64(23):1788–94.
[218] Lu S, Sui L, Liu J, Zhu S, Chen A, Jin M, et al. Near-Infrared Photoluminescent Polymer-Carbon Nanodots with Two-Photon Fluorescence. Adv Mater 2017;29(15):1603443.
[219] Liu Y, Li X, Zhang Q, Li W, Xie Y, Liu H, et al. A General Route to Prepare Low-Ruthenium-Content Bimetallic Electrocatalysts for pH-Universal Hydrogen Evolution Reaction by Using Carbon Quantum Dots. Angew Chem Int Ed 2020;59(4):1718–26.
[220] Liu Y, Yang Y, Peng Z, Liu Z, Chen Z, Shang L, et al. Self-crosslinking carbon dots loaded ruthenium dots as an efficient and super-stable hydrogen production electrocatalyst at all pH values. Nano Energy 2019;65:104023.
[221] Song H, Wu M, Tang Z, Tse JS, Yang B, Lu S. Single atom Ru doped CoP/CDs Nanosheets via Splicing of Carbon-Dots for Robust Hydrogen Production. Angew Chem Int Ed 2021.
[222] Li W, Liu Y, Wu M, Feng X, Redfern SAT, Shang Y, et al. Carbon-quantum-dots-loaded ruthenium nanoparticles as an efficient electrocatalyst for hydrogen production in alkaline media. Adv Mater 2018;30(31):e1800676.
[223] Li W, Wei Z, Wang B, Liu Y, Song H, Tang Z, et al. Carbon quantum dots enhanced the activity for the hydrogen evolution reaction in ruthenium-based electrocatalysts. Mater. Chem. Front. 2020;4(1):277–84.
[224] Li W, Liu Y, Wang B, Song H, Liu Z, Lu S, et al. Kilogram-scale synthesis of carbon quantum dots for hydrogen evolution, sensing and bioimaging. Chin. Chem. Lett. 2019;30(12):2323–7.
[225] Chandrasekaran P, Jebakumar Immanuel Edison TN, Sethuraman MG. Electrocatalytic performance of carbon dots/palladium nanoparticles composite towards hydrogen evolution reaction in acid medium. Int J Hydrogen Energy 2020;45(53):28800–11.
[226] Cardoso JASB, Šljukić B, Erdem M, Sequeira CAC, Santos DMF. Vine Shoots and Grape Stalks as Carbon Sources for Hydrogen Evolution Reaction Electrocatalyst Supports. Catalysts 2018;8(2).
[227] Yoon D, Seo B, Lee J, Nam KS, Kim B, Park S, et al. Facet-controlled hollow Rh_2S_3 hexagonal nanoprisms as highly active and structurally robust catalysts toward hydrogen evolution reaction. Energy Environ Sci 2016;9(3):850–6.
[228] Duan H, Li D, Tang Y, He Y, Ji S, Wang R, et al. High-Performance Rh_2P Electrocatalyst for Efficient Water Splitting. J Am Chem Soc 2017;139(15):5494–502.
[229] Liu Y, Hu X, Huang B, Xie Z. Surface Engineering of Rh Catalysts with N/S-Codoped Carbon Nanosheets toward High-Performance Hydrogen Evolution from Seawater. ACS Sustainable Chem Eng 2019;7(23):18835–43.
[230] Wang Q, Xu B, Xu C, Wang Y, Zhang Y, Wu J, et al. Ultrasmall Rh nanoparticles decorated on carbon nanotubes with encapsulated Ni nanoparticles as excellent and pH-universal electrocatalysts for hydrogen evolution reaction. Appl Surf Sci 2019;495.
[231] Liu S, Chen Y, Yu L, Lin Y, Liu Z, Wang M, et al. A supramolecular-confinement pyrolysis route to ultrasmall rhodium phosphide nanoparticles as a robust electrocatalyst for hydrogen evolution in the entire pH range and seawater electrolysis. J Mater Chem A 2020;8(48):25768–79.
[232] Ma J, Ma Z, Liu B, Wang S, Ma R, Wang C. Composition of Ag-WO_3 core-shell nanostructures as efficient electrocatalysts for hydrogen evolution reaction. J Solid State Chem 2019;271:246–52.
[233] Ji X, Liu B, Ren X, Shi X, Asiri AM, Sun X. P-Doped Ag Nanoparticles Embedded in N-Doped Carbon Nanoflake: An Efficient Electrocatalyst for the Hydrogen Evolution Reaction. ACS Sustainable Chem Eng 2018;6(4):4499–503.
[234] Zhou W, Xiong T, Shi C, Zhou J, Zhou K, Zhu N, et al. Bioreduction of Precious Metals by Microorganism: Efficient Gold@N-Doped Carbon Electrocatalysts for the Hydrogen Evolution Reaction. Angew Chem Int Ed 2016;55(29):8416–20.